Chemical Science

ROYAL SOCIETY OF CHEMISTRY

REVIEW

View Article Online
View Journal

Cite this: DOI: 10.1039/d5sc00569h

In situ Raman spectroscopic studies of CO_2 reduction reactions: from catalyst surface structures to reaction mechanisms

Dongao Zhang,[a] Xuan Liu,[a] Yu Zhao,[a] Hua Zhang, *[ab] Alexander V. Rudnev[c] and Jian-Feng Li *[ab]

The electrochemical CO_2 reduction reaction (eCO_2RR) has gained widespread attention as an important technology for carbon cycling and sustainable chemistry. *In situ* Raman spectroscopy, due to its molecular structure, sensitive advantage and real-time monitoring capability, has become an effective tool for studying the reaction mechanisms and structure–performance relationships in eCO_2RR. This article reviews recent advancements in the application of *in situ* Raman spectroscopy in eCO_2RR research, focusing on its critical role in monitoring reaction intermediates, analyzing catalyst surface states, and optimizing catalyst design. Through systematic studies of different catalysts and reaction conditions, *in situ* Raman spectroscopy has revealed the formation and transformation pathways of various intermediates, deeply exploring their relationship with the active sites of the catalysts. Furthermore, the review discusses the integration of *in situ* Raman spectroscopy with other characterization techniques to achieve a more comprehensive understanding of the reaction mechanisms. Finally, we summarize the current challenges and opportunities in this research area and look ahead to the future applications of *in situ* Raman spectroscopy in the field of eCO_2RR.

Received 22nd January 2025
Accepted 17th February 2025

DOI: 10.1039/d5sc00569h

rsc.li/chemical-science

1. Introduction

The overreliance on fossil fuels has given rise to numerous significant challenges, such as the greenhouse effect and rising sea levels. Therefore, how to convert renewable energy sources like solar energy into convenient forms for storage and transportation, as well as how to utilize renewable energy to reduce CO_2 concentrations, has become a pressing concern that requires immediate attention.[1–4] The electrochemical carbon dioxide (CO_2) reduction reaction (eCO_2RR) is one of the key

[a]College of Materials, College of Chemistry and Chemical Engineering, State Key Laboratory of Physical Chemistry of Solid Surfaces, College of Physical Science and Technology, Key Laboratory of High Performance Ceramics Fibers, Fujian Key Laboratory of Advanced Materials, College of Energy, Xiamen University, Xiamen 361005, China. E-mail: zhanghua@xmu.edu.cn; Li@xmu.edu.cn

[b]Innovation Laboratory for Sciences and Technologies of Energy Materials of Fujian Province (IKKEM), Xiamen 361102, China

[c]A. N. Frumkin Institute of Physical Chemistry and Electrochemistry, Russian Academy of Sciences, Leninsky Prospekt 31, 119071 Moscow, Russia

Dongao Zhang

Dongao Zhang obtained his bachelor's degree from Nanchang University in 2021 and is currently a PhD student at Xiamen University, under the guidance of Prof. Jian-Feng Li and Prof. Hua Zhang. His research focuses on the electrochemical CO_2 reduction reaction and in situ Raman spectroscopy studies.

Hua Zhang

Prof. Hua Zhang is a full Professor of College of Materials at Xiamen University. He obtained his PhD from Xiamen University in 2015 and worked as a post-doctor during 2015–2018 at Xiamen University. His research interests include heterogeneous catalysis, surface-enhanced Raman spectroscopy, and in situ spectroscopic (Raman/IR) methods for catalysis.

technologies for addressing global warming and the energy crisis. By electrochemically reducing CO_2, it can be transformed into valuable compounds like carbon monoxide (CO), formic acid (HCOOH), methanol (CH_3OH), and various hydrocarbons, thereby achieving carbon cycling and energy storage while reducing dependence on fossil fuels.[5–7] The eCO_2RR offers advantages such as environmental friendliness, ease of operation, and controllable product selectivity.[8]

Despite the enormous potential of eCO_2RR, its practical application still faces numerous challenges. CO_2 is a thermodynamically stable molecule, and its reduction reaction requires a high energy input.[9] Additionally, eCO_2RR involves multiple electron transfer processes, and different reduction pathways can yield various products. The nature of these products depends on the type of catalyst, reaction conditions (such as potential, pH, and temperature), and the composition of the electrolyte.[10] Furthermore, the kinetics of eCO_2RR is slow, especially in aqueous solutions, where the efficiency of eCO_2RR is often compromised by the competing hydrogen evolution reaction (HER).[11,12] In eCO_2RR, the design and optimization of electrocatalysts are central to achieving efficient conversion. An ideal electrocatalyst should not only exhibit high activity and reduce the overpotential for eCO_2RR but also possess high selectivity for specific products.[13,14] Additionally, the stability of the catalyst is a crucial indicator; the ideal catalyst should maintain its activity and structural stability over long reaction periods. Researchers have developed various electrocatalysts for eCO_2RR, including metal catalysts (such as copper, silver, gold, *etc.*), metal oxides (such as Cu_2O, SnO_2, *etc.*), carbon-based materials, as well as alloys and metal–organic frameworks (MOFs). Different catalysts exhibit varying selectivities in eCO_2RR.[15–20]

Despite the ongoing progress in the study of various electrocatalysts, the understanding of their active sites, reaction mechanisms, and surface intermediates during the reaction process remains insufficient.[21,22] This necessitates the use of advanced characterization techniques. *In situ* characterization techniques can dynamically monitor the structural changes of catalysts, the transformation processes of reactants, and the formation of intermediates during electrochemical reactions, providing vital information on the reaction mechanisms.[23–25] Commonly used *in situ* techniques include *in situ* Raman spectroscopy, *in situ* infrared spectroscopy, *in situ* X-ray absorption spectroscopy (XAS), and *in situ* transmission electron microscopy (TEM), *etc.* Among these *in situ* characterization methods, *in situ* Raman spectroscopy offers unique advantages by enabling real-time monitoring of catalyst surface structure changes and the formation of reaction intermediates under practical reaction conditions.[26,27] Raman spectroscopy is based on the scattering effect of molecular vibrational modes; when laser light interacts with molecules, some of the scattered photons undergo energy changes, resulting in characteristic Raman scattering spectra. By analyzing these spectra, information regarding molecular structures, bonding configurations, and their dynamic changes can be obtained, thereby revealing the essence of catalytic reactions and further guiding the optimization of catalyst design.[28,29] Raman spectroscopy is a non-contact, non-destructive optical characterization method with high selectivity, capable of distinguishing structurally similar molecules and studying low-frequency vibrational signals with relatively low sensitivity to water, making it suitable for research on chemical processes in aqueous solutions.[30–32]

Surface-enhanced Raman spectroscopy (SERS) is an exceptionally sensitive analytical method relying on the Raman scattering phenomenon. SERS significantly enhances Raman signals, greatly lowering the detection limits and enabling single-molecule detection.[33] The enhancement effect of SERS mainly depends on localized surface plasmon resonance (LSPR) occurring on the surface of noble metal (like Au, Ag, and Cu) nanostructures. By carefully designing nanostructures, SERS can dramatically increase the intensity of Raman scattering signals, making it widely applicable in trace substance detection, molecular recognition, and surface interface studies.[34] The electromagnetic enhancement mechanism is the main contributor to the SERS signal enhancement, typically increasing Raman signals by factors of 10^4 to 10^6. When laser light illuminates the surface of a metal with nanostructures, the free electrons at the metal surface interact with the optical field, resulting in LSPR and creating a strong electromagnetic field near the metal surface. Molecules adsorbed on the surface of metal nanostructures experience this localized enhanced electric field, leading to a significant increase in Raman scattering signals.[35] SERS technique has advantages such as high sensitivity and molecular specificity, but there are still some limitations in practical applications. Although SERS has expanded the application of Raman spectroscopy, it still faces two common issues: first, the limitation of substrate materials, as strong SERS effects can only be achieved on the surfaces of gold, silver, copper, and a few alkali metals; second, the limitation of surface morphology, as only rough or nanostructured metal surfaces exhibit high SERS activity, while smooth or single-crystal surfaces cannot be used for SERS studies.[36] Therefore, SERS technology has not been widely accepted by surface scientists for a long time. Our group developed shell-isolated nanoparticle-enhanced Raman spectroscopy (SHINERS),

Jian-Feng Li

Prof. Jian-Feng Li is a full Professor of Chemistry and the Vice Dean of College of Energy at Xiamen University. He received his BSc degree in Chemistry from Zhejiang University in 2003, and his PhD degree in Chemistry from Xiamen University in 2010. He worked as a post-doctor at University of Bern and ETH Zurich in Switzerland during 2011–2014. He is the senior editor of J. Phys. Chem. C His main research areas include surface-enhanced Raman spectroscopy, electrochemistry, interfacial catalysis, in situ characterization, and rapid Raman detection in public safety and health care.

wherein a very thin, dense inert silica shell was wrapped around gold nanoparticles, resulting in Au@SiO_2 core–shell structured nanoparticles or shell-isolated nanoparticles (SHINs).[37] By using SHINs as enhancement substrates, the SHINERS technique can significantly improve the detection sensitivity, even reaching the single-molecule level. This is crucial for the detection of low-concentration intermediates in eCO_2RR research. The SHINERS technique enables *in situ* detection under actual reaction conditions, which is of particular importance for eCO_2RR research. The traditional SERS technique may be interfered with in some complex reaction systems, while the SHINERS technique exhibits better adaptability. This method utilizes the strong electromagnetic field enhancement from the gold core nanoparticles to enhance the Raman signals of target molecules on the substrate materials. SHINERS has largely solved the problems of material and morphology generality in SERS.[38,39]

This article will review the latest advancements in *in situ* Raman spectroscopy within the field of eCO_2RR, focusing on its applications in revealing reaction mechanisms, identifying reaction intermediates, and studying the evolution of catalyst surfaces. Additionally, this article will discuss the current challenges facing this technology and explore potential future directions for improving the efficiency and selectivity of eCO_2RR.

2. Brief introduction of the development of eCO_2RR

The process of eCO_2RR begins with the adsorption of CO_2 onto the surface of the catalyst, followed by CO_2 activation. This is followed by multiple steps of electron transfer and proton coupling, generating various C_1 products and intermediates.[40] C–C coupling then occurs, resulting in the production of C_{2+} products such as ethanol and ethylene through further electron transfer and proton coupling.[41] Finally, the products desorb and diffuse away. However, the variety of intermediates and the complexity of the reactions make the mechanistic study of eCO_2RR challenging.[42] The activity and performance parameters of eCO_2RR include current density, faradaic efficiency (FE), energy efficiency (EE), and stability.[43,44]

2.1 Advance in catalysts

The development of catalysts is a core factor driving the advancement of eCO_2RR technology. As catalyst designing and optimization continue to progress, the efficiency and selectivity of eCO_2RR are significantly improving. Researchers have classified the differences in surface adsorption energies of *H and *CO among various single metal catalysts. Au, Ag, and Zn have relatively low adsorption energies for both *CO and *H, favoring the stabilization of *COOH intermediates, which leads to CO production. CO_2 undergoes proton-coupled electron transfer to generate the *COOH intermediate, which is then further reduced to CO. In contrast, In, Bi, Hg and Sn also have low adsorption energies, stabilizing *HCOO intermediates and resulting in HCOOH production. The direct reduction of CO_2 to formic acid involves the formation of the *OCHO intermediate. Metals such as Fe, Ni, Pd and Pt have higher adsorption energies for *H and *CO, leading to H_2 production, while Cu, with moderate adsorption energies, is the only single metal catalyst capable of producing multi-carbon products (Fig. 1a and b).[45,46] The reduction of CO_2 to C_{2+} products such as ethylene and ethanol involves C–C coupling steps and multiple proton–electron transfer steps. The adsorption and activation of CO_2 on the catalyst surface are the initial steps of the reaction. The formation and transformation of intermediates such as *COOH, *CO, and *OCHO are crucial for determining product selectivity. The efficiency and selectivity of the proton–electron transfer steps directly affect the final products.

To address the limitations of traditional single metal catalysts, researchers have begun developing alloy catalysts by combining two or more metals to modulate their surface properties and electronic structures.[47] Nanostructured catalysts, with their larger surface area and unique surface electronic characteristics, significantly enhance the activity of eCO_2RR.[48] These nanostructured catalysts can also improve the adsorption

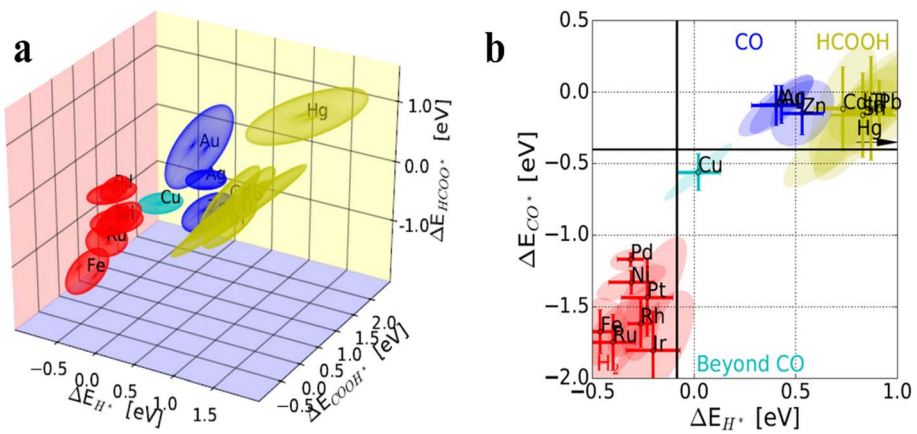

Fig. 1 (a) Coupled binding-energy ellipsoids of H*, HCOO*, and COOH* on diverse single metals. (b) Binding energies of the H* and CO* intermediates on diverse metal surfaces and their main products in eCO_2RR. (a) and (b) are reproduced from ref. 45 with permission from Wiley, copyright 2017.

of intermediates through surface structural regulation, surface engineering, and oxidation state adjustments, thereby modulating catalytic performance.[49] Furthermore, doping or functionalizing two-dimensional materials such as graphene and MoS_2, which have unique surface structures and electronic properties, optimizes their electrochemical performance, resulting in higher selectivity and product diversity in eCO_2RR.[50] Molecular catalysts such as metal phthalocyanines and porphyrin complexes can optimize the CO selectivity by adjusting the ligand structure, but they usually have poor stability. Metal–organic framework (MOFs) catalysts can regulate CO_2 adsorption and electron transfer pathways by combining different metal centres and organic ligands, optimizing the selectivity of reduction products. Covalent organic framework (COFs) catalysts exhibit excellent stability and conductivity, effectively promoting eCO_2RR, particularly in generating multi-carbon products.[51] Non-metal catalysts, such as nitrogen-doped carbon materials and carbon nanotubes, demonstrate excellent selectivity and activity in eCO_2RR, especially for producing CO and HCOOH. These materials are low-cost, abundantly available, and have good scalability and industrial application potential.[52] Single-atom catalysts (SACs) represent the latest development in catalyst technology, where individual metal atoms are dispersed on carbon-based materials or other substrates, offering high activity and selectivity.[53] These catalysts deliver exceptional performance with minimal metal usage and allow precise tuning of the electronic structure of active centres, further enhancing eCO_2RR efficiency.[54,55] Tandem catalysts, by combining two or more catalysts with different functions, can more effectively control reaction pathways, improve selectivity for complex products, suppress side reactions, reduce energy consumption, and enhance catalyst stability and longevity.[56,57]

2.2 Development of devices

The design and development of electrolyzers are key factors in improving reaction efficiency, selectivity, and industrial applications. The design of electrolyzers has evolved from simple laboratory-scale setups to more complex and efficient structures to meet industrial-scale application needs.[58,59] Traditional H-type electrolyzers consist of two isolated reaction chambers housing the cathode and anode, with ionic conduction between them facilitated by a proton exchange membrane, anion exchange membrane or salt bridge (Fig. 2a). Their simple structure makes them easy to operate and they are commonly used to explore the eCO_2RR performance, reaction mechanisms, and selectivity of different catalysts.[60] However, the poor solubility of CO_2 in liquid electrolytes limits the reaction due to constrained CO_2 supply, and the slow diffusion of gaseous products affects the overall reaction efficiency, making them unsuitable for high current densities and industrial applications.[61]

Flow cells utilize gas diffusion electrodes (GDE) to deliver gaseous CO_2 directly to the electrode surface (Fig. 2b). Unlike traditional H-type electrolyzers, GDEs allow CO_2 to enter the catalyst layer without first dissolving in the liquid electrolyte, thus improving the mass transfer rate of CO_2 and overcoming solubility limitations.[62,63] However, the design and manufacturing processes for the electrode structure are more complex, and the electrodes may become clogged by products during prolonged operation, reducing efficiency.[64] Membrane electrode assembly (MEA) electrolyzers, designed without liquid electrolyte at the cathode, address some issues of flow cells, such as overflow, impurity deposition on the catalyst surface, and carbonate crystallization, facilitating product separation (Fig. 2c). These designs offer high energy efficiency and compact configurations suitable for large-scale industrial applications, although the cost of electrolyte membranes and electrode materials remains high. Future electrolyzer designs will aim to further enhance energy conversion efficiency and reduce energy losses, especially in industrial applications.[65,66]

2.3 Development of characterization techniques for eCO_2RR

Developing characterization techniques for eCO_2RR is crucial for a deeper understanding of reaction mechanisms, catalyst performance, and reaction pathways.[67] Various advanced

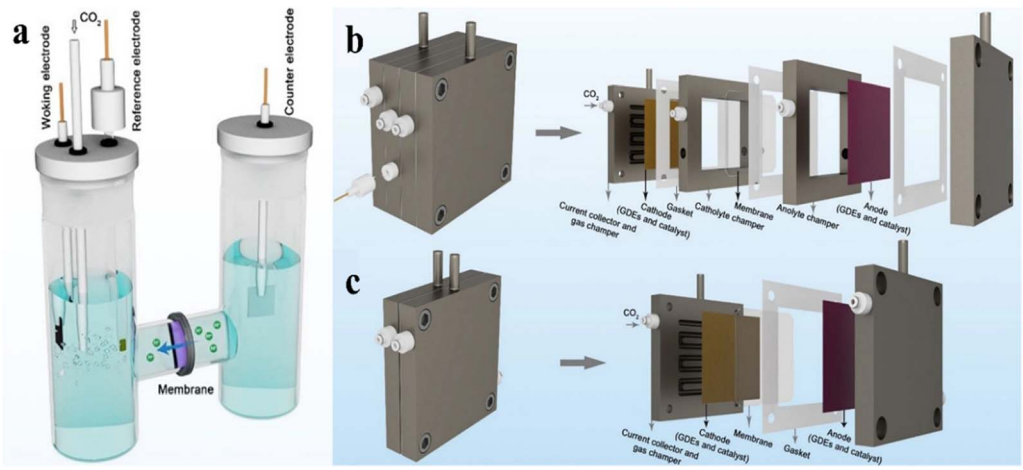

Fig. 2 Diagram of different types of eCO_2RR electrolytic cells. (a) H-type cell (b) flow cell (c) MEA. (a–c) are reproduced from ref. 59 with permission from Springer Nature Link, copyright 2023.

characterization methods are continuously introduced and refined to more accurately capture changes in the catalyst's structure, active sites, intermediates, and reaction products during the process.[68,69] Electrochemical characterization methods are fundamental tools for studying eCO_2RR processes and catalyst activities, providing key data such as current, potential, and efficiency. Linear sweep voltammetry (LSV) and cyclic voltammetry (CV) are used to investigate the redox characteristics of catalysts, determining the onset potential and overpotential for eCO_2RR.[70] Electrochemical impedance spectroscopy (EIS) measures charge transfer and resistance at the interface between the electrode and electrolyte, helping to understand mass transfer processes and charge transfer efficiency during the reaction.[71] *In situ* electron microscopy techniques, which combine electrochemical systems with electron microscopy, allow real-time observation of the morphology and structural evolution of electrocatalysts during eCO_2RR.[72] Online electrochemical mass spectrometry (OLEMS) is employed to analyze gaseous products formed during the reaction, such as methane (CH_4), CO, and H_2. OLEMS, combined with electrochemical testing, can monitor the generation of gas products in real time, providing information on faradaic efficiency and product selectivity.[73] Gas chromatography-mass spectrometry (GC-MS) is employed to analyze and quantify reaction products, particularly gaseous products (like CO and CH_4) and liquid products (such as HCOOH). By coupling gas chromatography with mass spectrometry, complex product distributions can be accurately identified and quantified. Nuclear magnetic resonance (NMR) serves as a characterization tool for liquid products, allowing precise analysis of formic acid, ethanol (C_2H_5OH), and other products formed in solution.[50,74]

The development of *in situ* spectroscopic techniques has greatly improved the ability to monitor reaction intermediates, changes in catalyst surface structures, and electronic states in real time during eCO_2RR.[75,76] *In situ* X-ray photoelectron spectroscopy (XPS) can simultaneously detect changes in the valence states of surface elements during eCO_2RR, revealing variations in active sites and catalyst reconstruction.[77] XPS mainly probes the information of several atomic layers on the sample surface. It is highly sensitive to the chemical composition and structure of the sample surface, enabling it to accurately reflect the true situation of the sample surface. Therefore, it is suitable for studying processes such as adsorption, catalysis, and oxidation on the material surface. *In situ* XAS, which includes X-ray absorption near-edge structure (XANES) and extended X-ray absorption fine structure (EXAFS), is used to probe the local structure of catalysts, changes in oxidation states, and the reconstruction of active sites during the reaction.[78] It is particularly effective for the analysis of transition metals and heavy elements, enabling the determination of information such as the types of elements, oxidation states, and coordination environments. *In situ* Fourier transform infrared spectroscopy (FT-IR) can detect intermediates and products formed during the reaction, particularly the vibrational modes of functional groups in intermediates like CO and COOH.[79,80] It can analyze almost all organic compounds and many inorganic compounds, including gas, liquid, and solid samples. *In situ* SERS enhances the intensity of Raman signals, allowing for real-time monitoring of surface intermediates formed during the reaction. The advantages of *in situ* SERS in eCO_2RR research include high sensitivity, real-time monitoring, molecular structure analysis, and direct characterization of catalyst surface states, as well as the ability to obtain information on low-frequency species. This makes SERS an important tool for studying the mechanisms of eCO_2RR, optimizing catalyst design, and understanding product selectivity, particularly in revealing complex reaction pathways and dynamic surface changes.[81,82] Usually, it does not require complex sample pretreatment and will not damage the sample. This makes it suitable for precious or fragile samples. Moreover, it can directly analyze samples in aqueous solutions, which is highly advantageous for studying reactions and substances in aqueous solutions in fields such as biochemistry and environmental science.

3. *In situ* Raman spectroscopic studies on non-Cu based catalysts

Non-Cu-based catalysts have several advantages in eCO_2RR. Firstly, they often exhibit higher selectivity, enabling the preferential generation of specific products, which broadens their application potential in synthesizing renewable fuels and chemicals.[52,83] Secondly, these catalysts demonstrate greater stability under reaction conditions, allowing them to function effectively over a wider range of potentials, thereby enhancing operational feasibility.[57,84] Additionally, the high availability and cost-effectiveness of non-Cu-based catalysts present considerable advantages.[85] Current research focuses on optimizing the structure and surface properties of these catalysts, exploring novel materials (such as MOFs and COFs), and improving reaction efficiency to advance the progress of non-Cu-based catalysts in the eCO_2RR field.[86–88]

3.1 Non-Cu metal and compound catalysts

Non-Cu metals and their compounds typically produce products such as CO and HCOOH in eCO_2RR. *In situ* Raman spectroscopy can not only monitor the changes of intermediates in the eCO_2RR but also analyze the changes in the catalyst surface state.[89] Jin's group *in situ* grew a $Bi@Bi_2O_3$ nanodendrite catalyst on Cu foil through a displacement reaction.[90] The *in situ* morphological reconstruction of $Bi@Bi_2O_3$ formed bismuth (Bi) nanoflowers, maximizing the exposure of active sites, thereby enhancing the adsorption and activation of CO_2. At a potential of −0.9 V *vs.* RHE, the FE for HCOOH reached 92.3%. *In situ* Raman spectroscopy of the eCO_2RR on this catalyst revealed, the emergence of a Raman peak at 1469 cm^{-1} after a period of reduction, corresponding to the *OCHO intermediate, and a peak at 1130 cm^{-1} corresponding to the *COOH intermediate (Fig. 3a). The *OCHO intermediate is a key precursor for formic acid, while the *COOH intermediate is crucial for CO production.[91]

Wang's group prepared a nanocomposite catalyst composed of bismuth clusters derived from a bismuth sulfide precursor

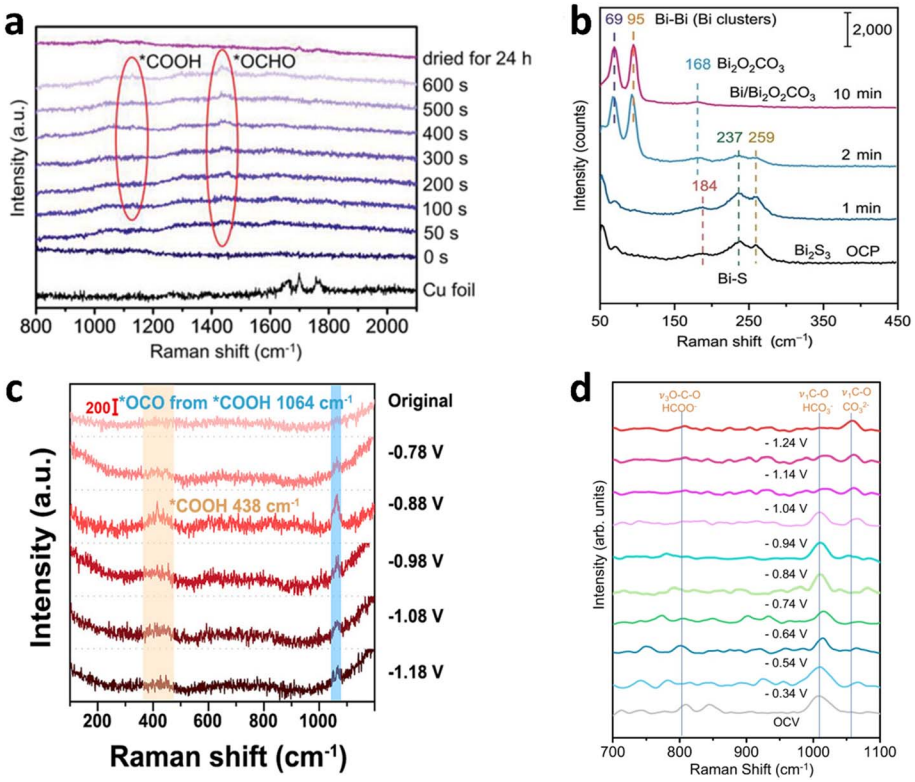

Fig. 3 (a) Time-dependent *in situ* Raman spectra recorded from the surface of Bi-NFs at −0.9 V *vs.* RHE; reproduced from ref. 90 with permission from Wiley, copyright 2023. (b) *Operando* Raman spectra of the Bi_2S_3-derived catalyst during eCO_2RR at various time at −0.75 V *vs.* RHE; reproduced from ref. 92 with permission from Wiley, copyright 2022. (c) *In situ* Raman spectra of s-PdNi/CNFs-1000 recorded between −0.78 and −1.18 V *vs.* RHE; reproduced from ref. 97 with permission from American Chemical Society, copyright 2022. (d) *In situ* Raman spectroscopic analysis on the intermediate adsorption for Sn–Bi at different potentials *vs.* RHE; reproduced from ref. 100 with permission from Springer Nature Link, copyright 2022.

and bismuth carbonate nanosheets ($Bi^0/Bi_2O_2CO_3$).[92] The catalyst achieved a current density of up to 2.0 A cm^{-2} in a flow electrolyzer for eCO_2RR, with a maximum FE for formate of 93%. With an energy conversion efficiency of 80% and a single-pass yield of 67% for formate, the system maintains stable operation for 100 hours at a current density relevant to industrial applications. *In situ* Raman spectroscopy revealed peaks at 259, 237, and 184 cm^{-1} corresponding to the B_{1g}, A_g, and A_g stretching modes of Bi–S bonds in Bi_2S_3 (Fig. 3b). With the reducing potential, these peaks gradually disappeared, followed by the emergence of Raman peaks at 168, 95, and 69 cm^{-1}. The peak at 168 cm^{-1} corresponds to the characteristic peak of $Bi_2O_2CO_3$, while the peaks at 95 and 69 cm^{-1} correspond to Bi–Bi vibrational bands.[93,94] The findings from *in situ* Raman spectroscopy, alongside *in situ* synchrotron radiation X-ray absorption spectroscopy and theoretical simulations, revealed that the bismuth atoms at the interface between the bismuth clusters and bismuth carbonate nanosheets serve as highly active sites under reaction conditions, enhancing formic acid production efficiency by promoting CO_2 activation and regulating the adsorption of the HCOO* intermediate. Through modifications of non-Cu metals, such as defect engineering and electronic structure adjustments, the derived compounds exhibit excellent electrocatalytic performance, particularly in selectivity, stability, and cost control. The structural changes of the catalyst may be more complex, making *in situ* Raman spectroscopy and other *in situ* characterization techniques necessary to reveal key information about the structural evolution and active sites of the catalyst.

3.2 Non-Cu metal alloy catalysts

By combining multiple metals, such as Ag–Pd, Au–Pt, and Ni–Fe, the electronic structure can be tuned to improve catalytic selectivity and activity.[95,96] Zhu's group prepared a PdNi alloy catalyst (s-PdNi/CNFs-1000) on CNFs in a carbon shell nanoreactor, and the s-PdNi alloy was synthesized by electrospinning Pd/Ni precursors with PVP in DMF, followed by graphitization, where the precursors decomposed, reduced metal clusters were confined in carbon nanofibers, and high-temperature diffusion enabled homogeneous alloy formation. The PdNi alloy catalyst achieved a maximum FE of 96.6% for CO at a potential of −0.88 V *vs.* RHE.[97] *In situ* Raman spectroscopy results during the eCO_2RR process revealed the peak at 1064 cm^{-1} corresponding to the *OCO asymmetric stretching from *COOH and the peak at 438 cm^{-1} corresponding to *COOH (Fig. 3c). The peak at 1064 cm^{-1} became sharp and intense at −0.88 V *vs.* RHE, and its intensity progressively decreased as the potential ranged from −0.88 to −1.18 V *vs.* RHE. This perfectly correlates with the s-

PdNi/CNFs-1000 catalyst, achieving its peak FE for CO of 96.6% at −0.88 V *vs.* RHE.[98,99] Chen's group designed an alloy material with a Sn–Bi bimetallic interface by *in situ* electrodeposition (ED) and evolution under CO_2RR conditions that exhibited high activity and stability, maintaining a maximum FE of over 90% for HCOOH production in the eCO_2RR across a wide potential window.[100] *In situ* Raman spectroscopy results during the eCO_2RR revealed the peak at 1010–1020 cm^{-1} corresponding to HCO_3^-, the peak at 1060–1070 cm^{-1} corresponding to CO_3^{2-}, and the peak at 796–802 cm^{-1} corresponding to $HCOO^-$ (Fig. 3d). As the potential became more negative, the peak for HCO_3^- gradually disappeared while the peak for CO_3^{2-} became dominant, possibly due to variations in the local pH.[101] The electronic configuration of the alloy catalyst is complex, and Raman spectroscopy helps to elucidate the modulation of intermediate adsorption strength by different metals, further optimizing catalytic performance.

3.3 Other non-Cu catalysts

Non-Cu-based catalysts also include various types, such as single-atom catalysts, MOFs, COFs, two-dimensional materials, and carbon-based catalysts. These materials can modulate the binding strength of key intermediates by altering the electronic or geometric structure of the active sites. They are cost-effective, abundant, and exhibit good scalability and potential for industrial applications. Liu's group constructed a nickel phthalocyanine molecule with a specific NiN_4 structure, which was then covalently linked to carbon nanotubes (CNTs) *via* a diazotization reaction to generate radicals (Fig. 4a).[102] The existence of Ni in a single-atom dispersed form was verified using aberration-corrected high-angle annular dark-field scanning transmission electron microscopy (HAADF-STEM) and X-ray absorption spectroscopy. Ultraviolet photoelectron spectroscopy revealed that some electrons on the CNT transferred to the NiN_4 active site. The eCO_2RR experiments showed that this material could selectively convert CO_2 to CO, achieving a maximum FE of up to 99%. The peaks at 182 and 244 cm^{-1} for nickel(II) 2,9,16,23-tetra(amino)phthalocyanine (Ni-TAPc) corresponded to isoindole deformation and Ni–N vibration. Under an Ar atmosphere, when the applied cathodic potential exceeded 0.57 V *vs.* RHE, the Ni–N peak shifted to lower wavenumbers, indicating a weakening of the Ni–N bond; after introducing CO_2, the Ni–N peak reverted to its initial shape and energy position (Fig. 4b and c). *In situ* Raman spectroscopy and synchrotron radiation characterization methods revealed Ni in Ni-TAPc was reduced during the eCO_2RR, and the *in situ*-formed Ni^+ was found to be highly effective in activating CO_2.[103,104]

Single-atom catalysts lead emerging catalytic technologies with their high atomic utilization and unique electronic effects; MOFs and COFs are important representatives of multifunctional catalytic materials due to their highly ordered pore structures and tunability; two-dimensional materials are widely applied in photocatalysis and electrocatalysis due to their excellent physical properties; and carbon-based catalysts hold broad application prospects due to their affordable cost, excellent conductivity, and strong stability. Future research will focus more on the synergistic effects of these materials and their multifunctional applications in different fields. *In situ* characterization techniques, such as *in situ* Raman spectroscopy, can help understand the structural changes, electronic variations, active sites, and intermediate changes of catalysts, guiding the synthesis strategies of these catalysts.[105–107]

4. SERS study of Cu-based catalysts

The application of Cu-based catalysts in the SERS study of eCO_2RR has received increasing attention in recent years. Compared to traditional noble metal (such as Au and Ag) based SERS active substrates, Cu-based catalysts exhibit unique potential in SERS research due to their low cost, abundant availability in the Earth's crust, and multifunctionality. In eCO_2RR, Cu can produce C_{2+} products due to its moderate adsorption of *H and *CO. However, the generation pathways for multi-carbon products like ethylene and ethanol are relatively complex, necessitating *in situ* characterization to monitor changes in intermediates in real time. This will deepen our insight into the reaction mechanisms of Cu-based catalysts in

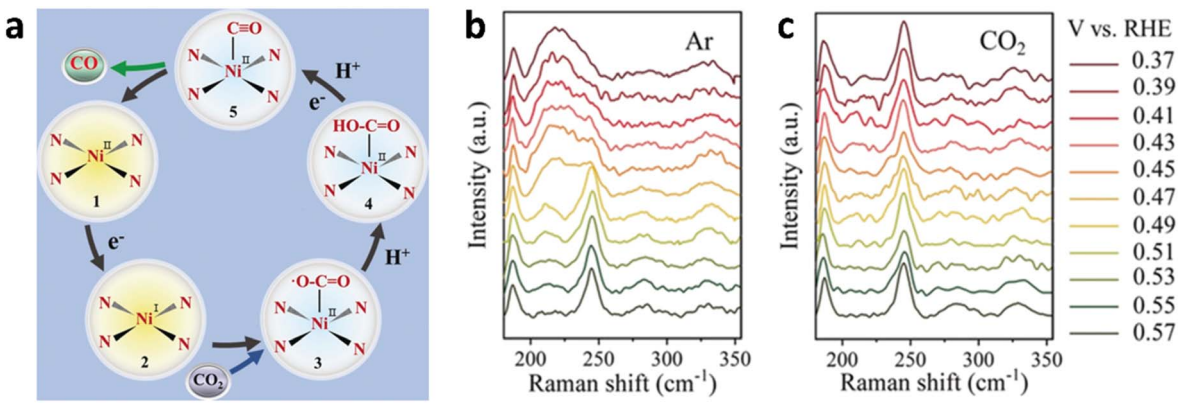

Fig. 4 (a) Proposed CO_2 reduction to CO pathway on the Ni SAC; Raman spectra of Ni-TAPc obtained on an Au electrode at different potentials (*vs.* RHE) in 0.5 M $KHCO_3$ aqueous solution at room temperature under (b) Ar and (c) CO_2 atmospheres. (a–c) Are reproduced from ref. 102 with permission from Wiley, copyright 2019.

eCO_2RR and provide further insights for designing catalysts that improve the selectivity and yield of high energy density C_{2+} products. SERS can provide insights into the local reaction environment by detecting surface-adsorbed water molecules, electrolyte ions, and intermediates. This is crucial for understanding how factors such as electric fields, solution pH, and electrode potential influence the reaction mechanisms.[108–110]

4.1 Single-crystal Cu electrodes

Single-crystal catalysts possess highly uniform surface lattice structures and orderly atomic arrangements, providing efficient active sites to enhance catalytic reaction efficiency. Moreover, their regular structures exhibit excellent stability, and the clear surface composition and structure facilitate in-depth exploration of reaction mechanisms and analysis of structure–activity relationships, driving catalyst design, development, and advancements in the field of catalysis.[36,111] Our group's recent work studied eCO_2RR on atomically smooth Cu(110) and Cu(111) single-crystal electrodes using *in situ* SHINERS.[112] As single-crystal Cu can not generate the SERS effect, we utilized the SHINERS technique to explore the reaction processes on single-crystal Cu electrodes by assembling $Au@SiO_2$ particles on their surface (Fig. 5a). The intense electromagnetic field produced by the plasmonic coupling between $Au@SiO_2$ and the substrate significantly enhanced the Raman signals of single crystal Cu, providing major insights into the reaction mechanisms of eCO_2RR. Direct spectral evidence of key eCO_2RR intermediates, such as $*CO_2^-$, *COOH, *CO, *OCCO, and $*CH_2CHO$, was captured on the surface of single crystal Cu(110). Based on *in situ* SHINERS and DFT results, it was

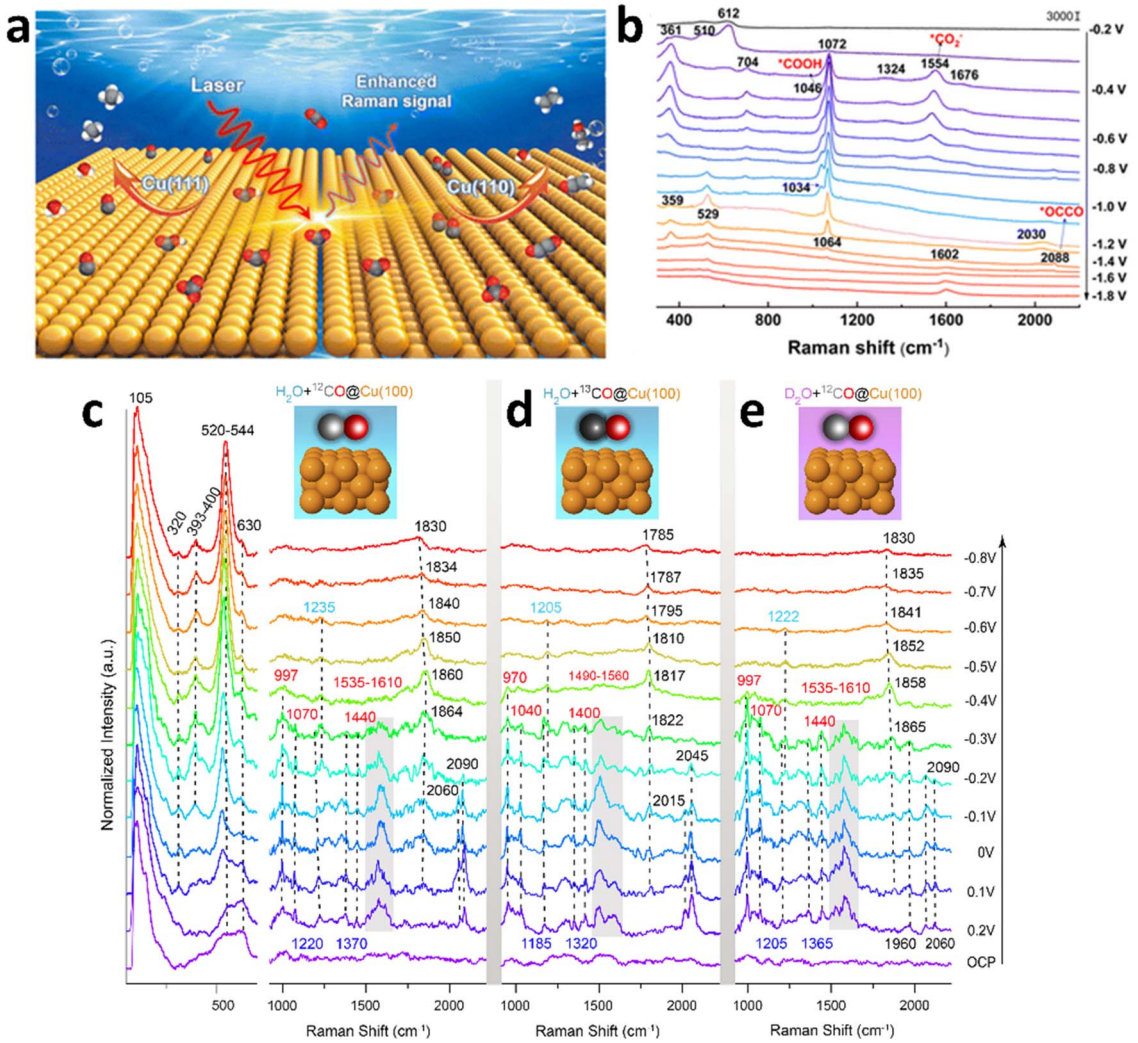

Fig. 5 (a) Diagrams illustrating the capture of intermediate species in eCO_2RR on Cu(111) and Cu(110) single-crystals by *in situ* Raman spectroscopy. (b) *In situ* Raman spectra of Cu(110) in a 0.5 M $KHCO_3/H_2O$ solution saturated with CO_2 at various potentials (*vs.* SCE). (a) and (b) are reproduced from ref. 112 with permission from The Royal Society of Chemistry, copyright 2022. (c–e) Potential-dependent EC-SHINERS spectra obtained from Cu(100) single-crystal in the presence of (c) ^{12}CO and (d) ^{13}CO and (e) with D_2O as electrolyte. The solutions were saturated with ^{12}CO or ^{13}CO gases and 0.1 M CsOH/OD electrolyte with a pH of 13. The Cu, ^{12}C, ^{13}C, and O atoms are depicted in orange, gray, black, and red colors, respectively. (c–e) are reproduced from ref. 116 with permission from the National Academy of Sciences of the United States of America, copyright 2022.

established that the CO_2RR process on the Cu(110) surface exhibited a high surface coverage of adsorbed *CO, promoting the formation of the *OCCO structure and the *CH_2CHO intermediate, which could lead to C_2 products (Fig. 5b). But the Cu(111) surface, with a lower *CO coverage, was found to be less favourable for the formation of the *OCCO structure, resulting in the production of primarily C_1 products.[113–115]

Lan's group combined SHINERS with *ab initio* molecular dynamics (AIMD) calculations to investigate the carbon monoxide reduction reaction (CORR) process on Cu single-crystal surfaces in different electrolytes (Fig. 5c–e).[116] The study focused on a pH = 13 electrolyte saturated with ^{12}CO, where C≡O stretching vibrations at 2060 cm^{-1} (on terrace sites) and 2090 cm^{-1} (on step sites) were detected on Cu(100) surfaces across a potential range from 0.2 V to −0.3 V (*vs.* RHE). Upon performing ^{13}CO isotope exchange, the C≡O stretching vibrations shifted to 2015 cm^{-1} and 2045 cm^{-1}, corresponding to the expected red-shift due to the difference in isotopic mass between ^{12}CO and ^{13}CO. The adsorbed *CO intermediates were rapidly reduced to hydrocarbons at more negative potentials. In addition, a set of Raman bands observed between 1830 and 1864 cm^{-1} were ascribed to C=O stretching modes of *CO intermediates on bridge sites of the Cu(100) surface.[117] These C=O vibrations exhibited a red-shift of approximately 44 cm^{-1} in the ^{13}CO labeling experiments, consistent with the mass-dependent vibrational frequency shift. Isotope substitution experiments and AIMD calculations revealed that the Raman peaks at 1220 cm^{-1} and 1370 cm^{-1} were assigned to the –C–OH bending mode and –C=C– stretching mode of the *HOCCOH intermediate on Cu(100). Under more negative potentials, the *HOCCOH intermediate was quickly consumed, leading to the disappearance of these Raman peaks. Additionally, peaks in the 1560–1610 cm^{-1} region were associated with the asymmetric stretching of *CO_2^- species, while peaks at 997 cm^{-1}, 1070 cm^{-1}, and 1440 cm^{-1} were assigned to surface-bound *CO_3^{2-} species. These peaks exhibited a red-shift in the ^{13}CO labeling experiments but remained unchanged during deuterium isotopic substitution, indicating that the species were in their deprotonated forms (*CO_2^- and *CO_3^{2-}) under strongly alkaline conditions. Finally, the peak at 520 cm^{-1} was assigned to O–H bending vibrations of surface-bound *OH species.[118]

4.2 Cu-based nanocatalysts

The catalytic activity of Cu-based nanocatalysts in CO_2 electroreduction is influenced by various factors. In terms of morphology, different nanostructures, such as particles, wires, and sheets, play distinct roles in activity, selectivity, and stability due to differences in specific surface region, active sites exposure, and mass transport properties. Regarding valence states, the electronic structure and chemical properties of Cu^0, Cu^+, and Cu^{2+} differ, with Cu^+ being critical for activity and selectivity toward C_{2+} products, while the stability of valence states affects long-term performance. Crystal facets exhibit variations in surface energy, atomic arrangement, and electronic structure, which influence CO_2 adsorption, activation, and product selectivity, and their stability can also change during the reaction. Defects alter the surface electronic structure and chemical properties, and an appropriate amount can enhance activity and selectivity. In summary, these factors are interrelated and collectively affect the overall performance of Cu-based nanocatalysts in CO_2 electroreduction.

The research group led by Cuenya prepared Cu electrodes using electrochemical oxidation-reduction methods, with X-ray diffraction results confirming the presence of Cu in the form of Cu_2O.[119] *In situ* SERS results indicated that at open circuit potential, characteristic peaks of Cu_2O appeared at 400, 528, and 620 cm^{-1} (Fig. 6a). As a reducing potential was applied, Cu_2O was reduced to metallic Cu, and peaks at 1390 and 1610 cm^{-1} corresponded to the symmetric and asymmetric stretching vibrations modes of *COOH. Peaks at 280, 355–360, and 1970–2110 cm^{-1} corresponded to the restricted rotation of adsorbed CO, Cu–CO stretching, and C–O stretching, respectively. Peaks in the range of 490–530 cm^{-1} were attributed to Cu–O or Cu–C stretching. As the reducing potential became more negative, the CO coverage increased, leading to the disappearance of peaks at 1390 and 1610 cm^{-1}, with new peaks appearing at 1450 and 1550 cm^{-1} corresponding to the *OCCO intermediate. As the potential was further decreased, the CO coverage continued to increase, revealing four new peaks at 1182, 1318, 1453, and 1595 cm^{-1} corresponding to the CCO symmetric stretching, CCO antisymmetric stretching, C–C stretching, and C–O (or C=C) stretching of *$OCHCH_2$ (or *$OCHCH_3$), which showed systematic changes with the potential. The peak in the range of 2830–2990 cm^{-1} was attributed to C–H stretching.[120,121] A new reaction mechanism scheme for eCO_2RR to C_{2+} was proposed through *in situ* SERS characterization combined with DFT simulations, which clearly linked active sites, reaction intermediates, and product selectivity (Fig. 6b).

Bao's group developed a carbon-coated CuO_x (CuO_x@C) catalyst which was fabricated through one-pot pyrolysis of a Cu-based metal–organic framework (MOF) in a tube furnace with air as carrier gas. This synthesis approach enabled the catalyst to exhibit high selectivity for the electroreduction of CO_2 to ethanol with a faradaic efficiency of 46%.[122] To elucidate the role of the carbon coating, *operando* Raman spectroscopy was performed using a custom-designed cell, revealing key insights into the catalytic mechanism. When current was applied to both CuO_x@C and CuO_x catalysts, Raman peaks at 291 and 610 cm^{-1}, corresponding to CuO, were disappeared (Fig. 6c and d). Instead, a new Raman peak emerged at 532.3 cm^{-1} on CuO_x@C, attributed to the presence of Cu^+ species.[123] Notably, Cu^+ species in CuO_x@C were stabilized across a wide range of current densities, a behavior not observed in CuO_x. Additionally, on both catalysts, an adsorbed *CO intermediate was detected at a wavenumber of 364.3 cm^{-1}. This *CO intermediate is acknowledged as a crucial intermediate in the formation of C_{2+} products. As the current density increased, the adsorbed *CO intensity exhibited a more rapid decline on CuO_x@C compared to that on CuO_x. This behavior is likely because of the higher ratio of Cu^+ species in CuO_x@C, which facilitates the conversion of *CO into C_{2+} products through C–C coupling. The carbon coating was found to play a pivotal role in stabilizing Cu^+

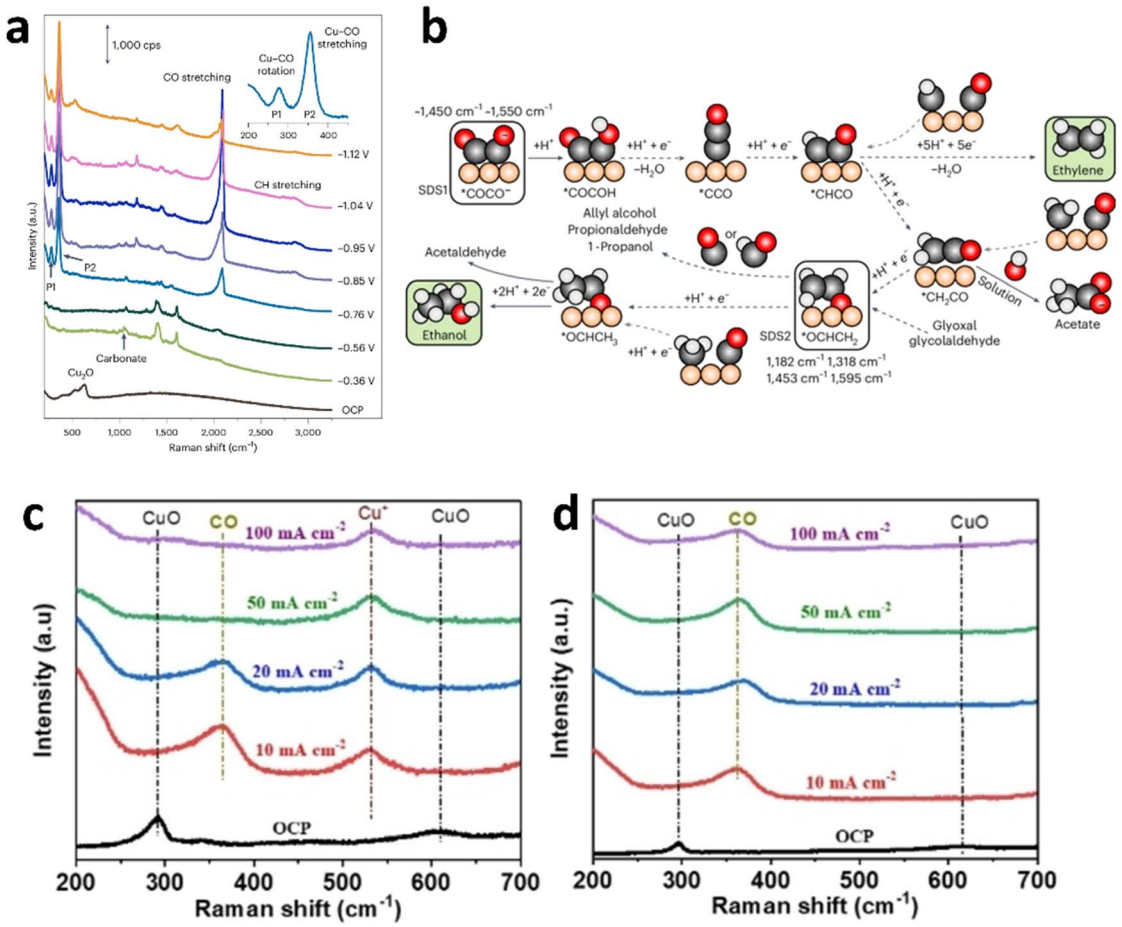

Fig. 6 (a) Raman spectra obtained from electrochemically treated Cu foil during eCO_2RR within potentials range from the open-circuit potential (OCP) to about −1.1 V *vs.* RHE in a 0.1 M $NaClO_4$ electrolyte that had been saturated with CO_2 gas. (b) Proposed reaction scheme for the generation of ethylene and ethanol. (a) and (b) are reproduced from ref. 119 with permission from Springer Nature Link, copyright 2024. *Operando* Raman spectra analysis during CO_2RR at varying current densities. (c) CuO_x@C. (d) CuO_x. (c) and (d) are reproduced from ref. 122 with permission from Wiley, copyright 2022.

species during the CO_2RR, while also enriching the concentrations of molecules taking part as reactants and the intermediate entities existing in the microenvironment of the reaction. Moreover, the carbon layer improved the electronic conductivity of the CuO_x@C catalyst, enabling efficient electron transfer passing from the circuit outside to the surface of the catalyst material. This enhancement suppressed the self-reduction of CuO_x species and promoted the timely conversion of reactant molecules, further contributing to the formation of C_{2+} products. These findings highlight the synergistic effects of carbon skin and Cu^+ species stabilization in enhancing the catalytic activity of CuO_x@C for CO_2RR.

By implementing heteroatom engineering on Cu-based catalysts, Qiao's group achieved reliable ampere-level electrolysis for converting CO_2 into C_{2+} products. A range of Cu-based precursor catalysts incorporating various non-metallic dopants (nitrogen, phosphorus, sulfur, oxygen) were fabricated through a single-step thermal decomposition process in an inert argon environment. Upon the introduction of heteroatoms (N, P, S, O), the Cu compounds experienced substantial structural reconstruction under the conditions of the CO_2 reduction reaction, forming heteroatom-derived Cu with enhanced catalytic properties.[124] To gain deeper insight into the local catalytic environment and evaluate HER competition, *in situ* SERS was employed (Fig. 7a–c). Signals at 1012 cm^{-1} and 1065 cm^{-1} were attributed to adsorbed HCO_3^- and CO_3^{2-} species, respectively.[125] These adsorbed species were detected on N–Cu, O–Cu, and Cu catalysts as the applied potential became increasingly negative. Notably, the HCO_3^-/CO_3^{2-} ratio on N–Cu exhibited a volcano-shaped trend with increasing potential, suggesting an optimal balance of local proton concentration. In contrast, this ratio decreased monotonously for O–Cu and was invalid for Cu due to signal shielding caused by surface gas formation. The HCO_3^-/CO_3^{2-} ratio served as an indicator of the local proton concentration around the catalysts during eCO_2RR. A higher ratio signified a higher proton concentration, revealing that local proton consumption on N–Cu was slower compared to Cu and O–Cu. This slower consumption indicated suppressed HER activity on N–Cu, while Cu and O–Cu showed more pronounced HER competition as H

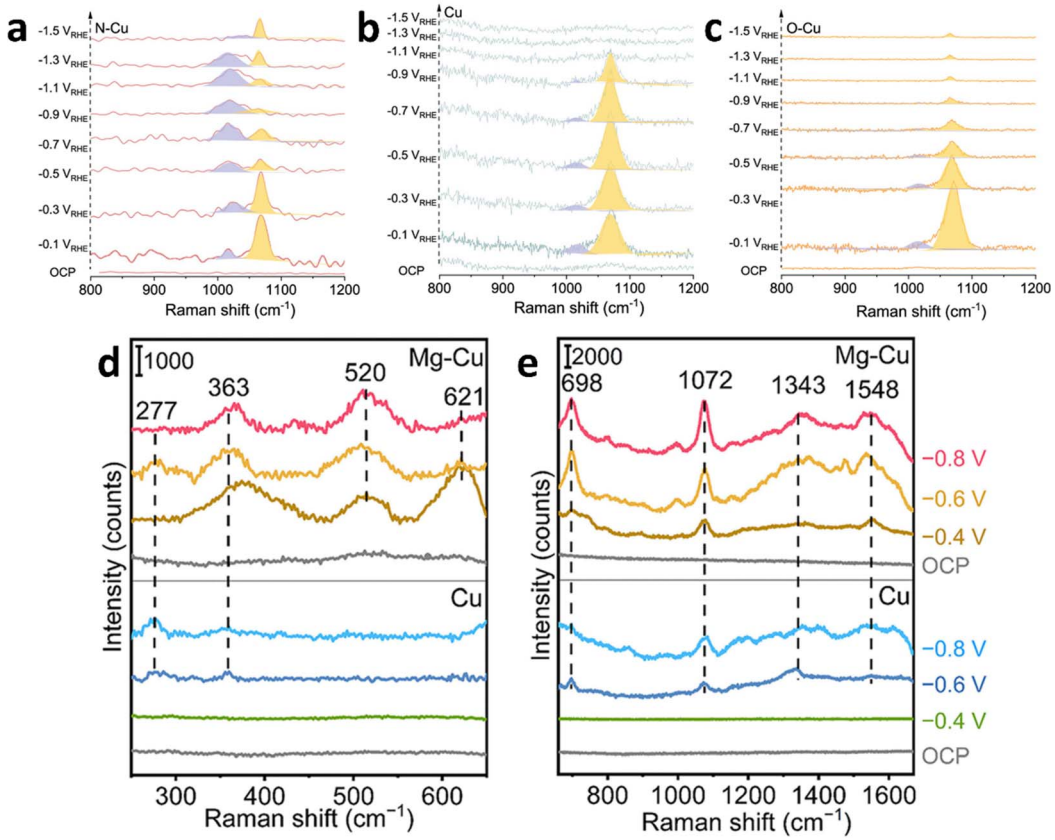

Fig. 7 *In situ* SERS of different Cu-based catalysts under CO_2RR conditions. (a) N–Cu; (b) Cu; (c) O–Cu. (a)–(c) are reproduced from ref. 124 with permission from American Chemical Society, copyright 2022. (d) Low energy region and (e) high energy region of *in situ* Raman spectra for Cu and Mg–Cu within a CO_2-saturated 0.5 M $KHCO_3$ electrolyte at various potentials (V *vs.* RHE). (d) and (e) are reproduced from ref. 128 with permission from Wiley, copyright 2022.

proton consumption increased. Density functional theory (DFT) calculations further confirmed that N–Cu exhibited a higher adsorption strength for *CO. Such enhanced *CO adsorption occurred at both the bridge and atop sites of Cu, which led to the suppression of HER and a significant decrease in the energy barrier for C–C coupling. These combined effects underscore the superior catalytic performance of N–Cu for CO_2-to-C_{2+} electrolysis.

Introducing other metal elements (such as Ag, Au, Zn, Pd, *etc.*) onto the surface of Cu can form bimetallic or alloy catalysts. This modification usually changes the electronic structure of Cu, thereby enabling the regulation of reaction intermediates that are adsorbed on the catalyst's surface. The introduction of different metals can finely tune the selectivity for various products, making Cu-based catalysts a highly promising material system in the field of eCO_2RR.[126,127] Wang's group discovered a magnesium (Mg)-modified Cu catalyst for eCO_2RR to C_{2+} products using an automated high-throughput screening platform.[128] The bimetallic Cu–Mg catalytic materials were synthesized through a facile reduction approach employing sodium borohydride as the reducing agent. This catalyst achieved a maximum FE of 80% for C_{2+} products at a current density of -1 A cm^{-2}. *In situ* SERS results of eCO_2RR revealed that even at -0.8 V *vs.* RHE, the Mg–Cu catalyst still showed characteristic peaks of Cu_2O at 520 and 621 cm^{-1}, which were absent in the Cu catalyst, indicating the introduction of Mg stabilizes Cu^+ during the eCO_2RR process (Fig. 7d and e). At -0.4 V *vs.* RHE, the Mg–Cu catalyst spectrum exhibited Raman peaks at 698, 1343, and 1548 cm^{-1}, corresponding to the umbrella motion of the oxygen atoms in the $*CO_2^-$ intermediate, symmetric C–O stretching, and asymmetric C–O stretching, respectively. A Raman peak at 1072 cm^{-1} corresponded to the C–O symmetric stretching of CO_3^{2-} in the electrolyte, with lower intensity and more negative potential in the Cu catalyst. Additionally, the Mg–Cu catalyst showed Raman peaks at 277 and 363 cm^{-1}, corresponding to frustrated rotation and stretching vibrations of Cu–CO, with stronger stretching vibration intensity in the Mg–Cu catalyst compared to the Cu catalyst, indicating a broader surface coverage of *CO.[113,125] This indicated that the addition of Mg facilitated the activation of CO_2 on the Cu surface, thereby generating the crucial intermediate *CO required for C–C coupling.

4.3 Single-atom Cu catalysts

The advantages of single-atom catalysts (SACs) in eCO_2RR mainly include high atomic utilization, unique active sites, enhanced selectivity for multi-carbon products, reduced overpotential, and suppression of hydrogen evolution reactions.

Through synergistic interactions with the support, Cu SACs can effectively optimize the reaction pathways and adsorption behaviors of intermediates in eCO_2RR, demonstrating excellent performance in generating high-value-added chemicals (such as C_{2+} products). Han's group had developed a silica-mediated hydrogen-bonded organic framework templating approach for fabricating a high-density single-atom copper catalyst with Cu–N_3 sites supported on thin-walled N-doped carbon nanotubes.[129] This catalyst, denoted as TWN-$Cu_{13.35}$-600-SACs, achieved an impressive copper loading of 13.35 wt%. In an H-type electrolyser, it demonstrated exceptional performance, achieving a maximum FE of 81.9% for ethanol production at a partial current density of 35.6 mA cm^{-2}. *In situ* SERS measurements during the electrochemical CO_2 reduction reaction (eCO_2RR) provided key insights into the reaction mechanism (Fig. 8a and b). At open circuit potential, peaks in the range of 200–400 cm^{-1} were attributed to the presence of Cu–N_3 sites, while the peak at 1167 cm^{-1} was associated with carbonate species. Upon applying potentials from −0.8 to −1.0 V *vs.* RHE, the peaks at 293 cm^{-1} and 351 cm^{-1} were assigned to the frustrated rotation of C=O and the stretching vibration of Cu–CO, respectively. The peak at 2010 cm^{-1} corresponded to the low-frequency band of linearly adsorbed CO* at the Cu–N_3 site, whereas the peak at 2060 cm^{-1} represented the high-frequency band of linearly adsorbed CO*. As the potential was further shifted from −1.0 to −1.3 V *vs.* RHE, the peak at 2010 cm^{-1} shifted to 2042 cm^{-1} due to the electrochemical Stark effect, caused by interactions between the applied electric field and the top-adsorbed CO molecules. In contrast, the peak at 2060 cm^{-1} shifted slightly to 2090 cm^{-1}, with minimal change in the chemical bond strength. This indicated that CO* at the top of the Cu site exhibited a higher propensity for C–C coupling, thereby driving the ethanol production pathway effectively.[130]

Wang's group successfully achieved the construction of the first Cu–C chemical bond in graphdiyne (GDY) by rationally designing and *in situ* anchoring copper single atoms (Cu-SAs) onto a unique GDY platform. The atomically dispersed copper catalysts supported on graphdiyne (Cu/GDY) were fabricated *via* an integrated adsorption-reduction strategy. This innovative strategy resulted in a remarkable FE of 81% and excellent stability for the electrochemical CO_2 reduction reaction (eCO_2RR) to CH_4.[131] Raman spectra of pristine GDY exhibited four characteristic peaks corresponding to the D band, G band, and the vibrational modes of conjugated diacetylene bonds (Fig. 8c and d). Upon anchoring Cu-SAs onto GDY, the vibrational peaks of the conjugated diacetylene units shifted positively from 1933 and 2174 cm^{-1} to 1945 and 2185 cm^{-1}, respectively, confirming the formation of Cu–C bonds. Moreover, the extended X-ray absorption fine structure (EXAFS) spectrum revealed a prominent peak at 1.48 Å, attributed to the Cu–C bond, but without Cu–Cu coordination peak around 2.2 Å.

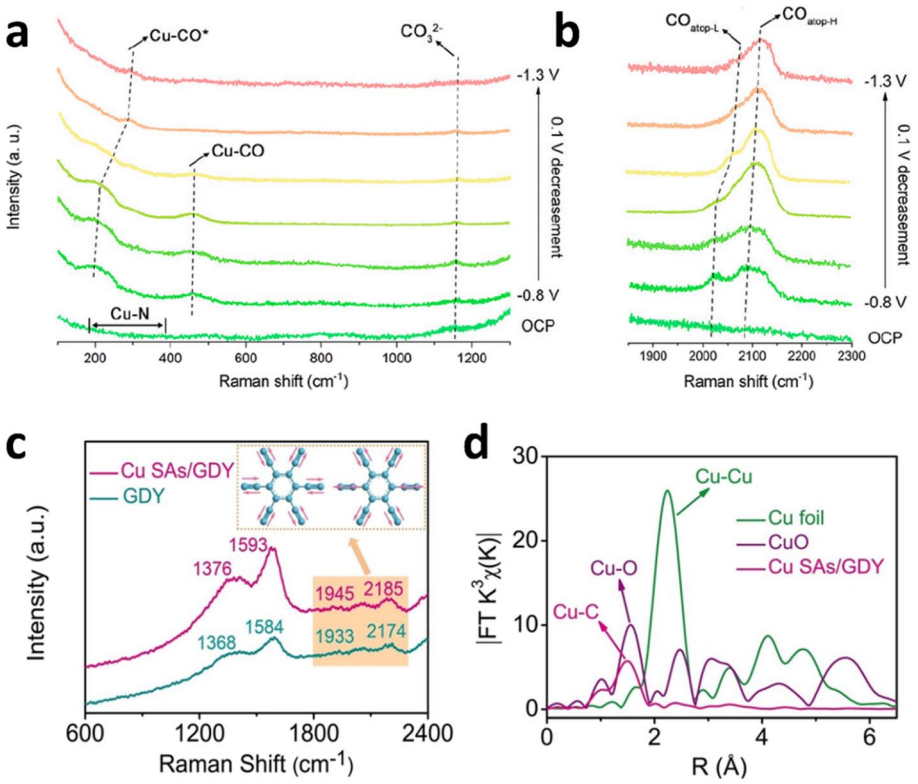

Fig. 8 *In situ* electrochemical SERS measurements for (a) low energy region and (b) high energy region for TWN-$Cu_{13.35}$-600-SACs during the eCO_2RR. (a) and (b) are reproduced from ref. 129 with permission from American Chemical Society, copyright 2023. (c) Raman spectra of pure GDY and Cu SAs/GDY. (d) FT EXAFS spectra of Cu SAs/GDY and Cu foil. (c) and (d) are reproduced from ref. 131 with permission from Wiley, copyright 2022.

This indicates that the Cu atoms are predominantly present in the form of isolated atoms in Cu SAs/GDY. Comprehensive characterization using techniques such as XAS, XPS, and Raman spectroscopy, combined with DFT simulations, further demonstrated that the Cu–C bond in Cu SAs/GDY not only facilitated effective charge transfer but also played a critical role in controlling reaction intermediates. Specifically, it promoted the formation of the *OCHO intermediate and guided a more advantageous reaction route for CH_4 production, thereby significantly enhancing catalytic efficiency.[132,133]

4.4 Other Cu-based tandem catalysts

Cu-based tandem catalysts exhibit significant advantages in eCO_2RR, particularly in generating multi-carbon products, optimizing reaction pathways, and enhancing catalyst stability. Through the synergistic effects of different functional materials, tandem catalysts can significantly improve the efficiency and selectivity of eCO_2RR, providing important pathways for developing efficient, stable, and tunable CO_2 reduction technologies. Zhang's group constructed a Cu^0–Cu^I tandem catalyst, Cu^0@PIL@Cu^I-5, based on polymer ionic liquids (PIL).[134] The fabrication of poly(ionic liquid)-stabilized Cu^0–Cu^I nanocomposites involved a sequential synthetic approach: initially, the Cu nanoparticle-embedded polymeric framework was constructed through *in situ* polymerization of vinyl-functionalized ionic liquid monomers, followed by the incorporation of CuCl *via* solution impregnation. During the eCO_2RR, the interfaces derived from Cu nanoparticles (Cu^0-PIL) and Cu^I species (PIL-

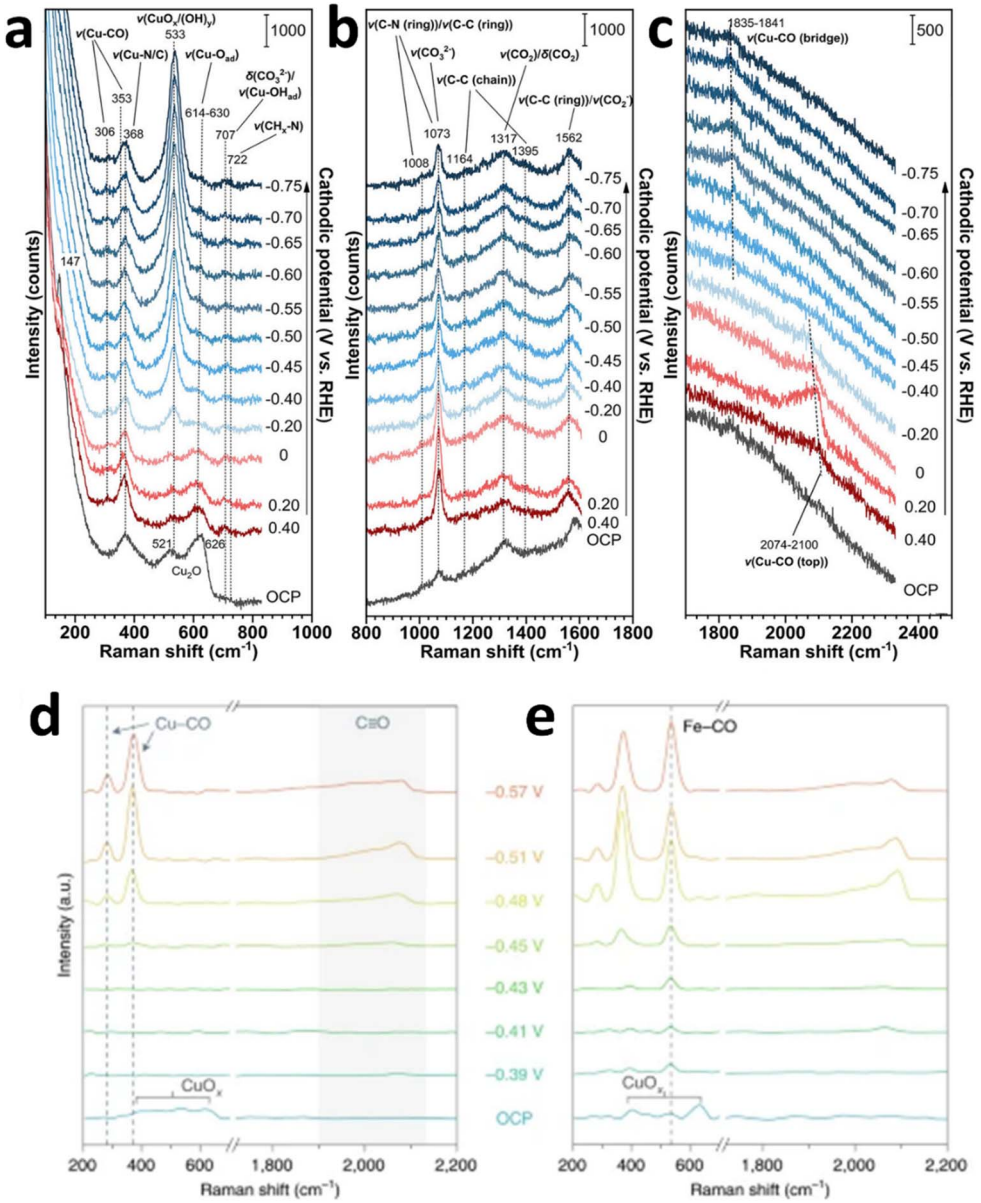

Fig. 9 (a–c) *In situ* Raman spectra obtained on GDE loaded with Cu^0@PIL@Cu^I-5 at various cathodic potentials across different Raman shift ranges. (a)–(c) are reproduced from ref. 134 with permission from Wiley, copyright 2021. *In situ* Raman spectra of the Cu (d) and FeTPP[Cl]/Cu (e) catalysts under varying applied potentials. (d) and (e) are reproduced from ref. 137 with permission from Springer Nature Links, copyright 2020.

Cu^{I}) exhibited a tandem effect, achieving a maximum FE of 76.1% for C_{2+} products, with a partial current density of 304.2 mA cm^{-2}. *In situ* Raman results for the eCO_2RR with Cu^{0}@PIL@Cu^{I}-5 indicated that when the cathodic potential started from 0 V *vs.* RHE, the peaks of Cu_2O at 521 and 626 cm^{-1} gradually diminished, while the peaks at 306 and 353 cm^{-1} corresponded to Cu–CO on Cu. Within the potential interval from −0.2 to −0.75 V *vs.* RHE, characteristic peaks of CuO_x and Cu $(OH)_y$ appear (Fig. 9a–c). The Cu–N/C peak at 368 cm^{-1} did not change with the potential. Peaks at 1008, 1073, 1164, 1317, 1395, and 1562 cm^{-1} were attributed to the PIL framework. As the potential became more negative, the Cu–CO (top) peak at 2100 cm^{-1} gradually disappeared, indicating a rapid reduction kinetics of *CO. Combined with DFT calculations and other characterization methods, the feeble interactions between the PIL units and the reaction intermediates facilitated the reduction of the energy barrier for C–C coupling, thereby increasing the selectivity for C_{2+} products.[135,136]

Sargent's group proposed a synergistic catalyst design at the molecular–metal interface, aimed at creating a localized environment abundant in reaction intermediates to improve the performance of electrochemical synthesis of ethanol from CO_2 and H_2O.[137] This approach was realized through the modification of the copper surface using a range of porphyrin-derived metal complexes. The porphyrin metal complex 5,10,15,20-tetraphenyl-21H,23H-porphine iron(III) chloride (FeTPP[Cl]) was shown to catalyze the conversion of CO_2 to CO. The FeTPP[Cl]/Cu catalyst achieved a maximum FE of 41% for converting CO_2 to ethanol, with a partial current density of 124 mA cm^{-2} at −0.82 V *vs.* RHE. *In situ* Raman spectra of eCO_2RR indicated that as the reduction potential is applied, the peaks corresponding to surface oxidized copper gradually disappeared (Fig. 9d and e). On the bare Cu electrode, three peaks associated with surface-adsorbed *CO were found in the range of 280, 365, and 1900–2130 cm^{-1}, corresponding to frustrated rotation, stretching vibrations of Cu–CO, and C≡O stretching, respectively. A new peak at 535 cm^{-1} was also observed on the FeTPP[Cl]/Cu catalyst electrode, attributed to the bending vibration of Fe–CO resulting from the interaction between Fe in the porphyrin and CO.[138] Further *in situ* Raman spectroscopy combined with XAS and DFT simulations demonstrated that FeTPP[Cl] catalyzed the conversion of CO_2 to CO, which then accumulated at nearby Cu sites for C–C coupling to produce ethanol and other products.

5. Conclusions and prospects

Significant progress has been made in the study of SERS in eCO_2RR over the past few years. As a highly sensitive surface analysis tool, SERS provides *in situ* monitoring of the reaction intermediates, products, and the surface state of catalysts during the eCO_2RR process, helping to deepen the understanding of reaction mechanisms, active sites, and the structure–performance relationships of catalysts.[139–141] In complex reaction systems, there may be fluorescence backgrounds, non-specific adsorption, or solvent signals, which interfere with the detection of the target Raman signals. The enhancement effects of SERS substrates on different species are inconsistent, which may cause the target signal to be masked or distorted. During long-term reactions, SERS substrates may experience signal attenuation due to contamination, oxidation, or structural changes. In the future, advancements in SERS will continue in areas such as high temporal and spatial resolution, the development of non-precious metal substrates, and integration with theoretical calculations, driving the development of efficient, low-cost and stable eCO_2RR catalysts. It is necessary to develop time-resolved Raman or surface-selective enhancement techniques to separate the target signal from background interference. The combination of *in situ* Raman with techniques such as XAS or mass spectrometry (MS) provides multi-dimensional reaction information. The development of the combined *in situ* Raman and atomic force microscopy (AFM) technique enables the simultaneous acquisition of chemical information and surface morphology. Combined with machine learning algorithms, the automatic analysis of Raman spectra and prediction of reaction pathways can be achieved, which may lead to the development of a high-throughput Raman detection platform to accelerate catalyst screening and reaction optimization. This will provide crucial technological support for the resource utilization of CO_2 and achieving carbon neutrality goals.[142–144]

5.1 Improvement of temporal and spatial resolution

Enhancing the temporal and spatial resolution of SERS technology is crucial for *in situ* monitoring the generation and transformation processes of rapidly forming reaction intermediates. By developing faster time-resolved Raman techniques, transient intermediates can be captured, revealing complex reaction kinetics. The advancement of ultrafast time-resolved SERS technologies, such as femtosecond SERS, will aid in studying transient species and ultrafast reaction dynamics during the reaction process. Combining these techniques with scanning probe technologies or other nanoscale imaging methods will allow for nanoscale spatial resolution SERS to analyze the activity differences across various regions of the catalyst surface.

5.2 Integration of multiple techniques

SERS can be combined with other *in situ* imaging techniques (such as electrochemical microscopy and electron microscopy) for multidimensional characterization of the reaction system. By integrating SERS with electrochemical scanning electron microscopy (SECM) and electrochemical transmission electron microscopy (TEM), the relationship between the microscopic structural changes on the catalyst surface and reaction activity can be observed at the molecular level. Combining electrochemical *in situ* SERS with X-ray absorption spectroscopy and scanning tunneling microscopy (STM) can facilitate the study of catalyst structural evolution and reaction mechanisms at the atomic scale. Full-spectrum SERS imaging technology can reveal the reaction activity of different regions on the catalyst surface, helping to understand the impact of surface heterogeneity on catalytic activity.

5.3 Development of new SERS active substrates

The performance of SERS depends on the Raman enhancement effect of the substrate. In the future, new SERS active substrates, especially novel materials like two-dimensional materials and single-atom catalysts, can be developed to enhance SERS sensitivity and resolution. Notably, the selectivity and enhancement effects of SERS substrates can be further optimized based on these new materials. For example, combinations of materials like graphene and nitrogen-doped carbon with metallic nanostructures may provide stronger enhancement effects while suppressing background signal interference. Developing non-precious metal SERS substrates (such as Cu or Ni substrates) can reduce costs and broaden the application range of SERS.

5.4 Mechanistic studies of multi-electron transfer reactions

eCO_2RR involves complex multi-electron transfer processes and various reaction pathways. In the future, SERS technology can be further employed to explore the reaction mechanisms of these multi-electron transfer reactions in depth, particularly by integrating DFT calculations to elucidate the key steps and energy barriers of electron transfer, and to predict and explain the relationship between Raman shifts observed in SERS experiments and the structures of intermediates, thereby enhancing the understanding of reaction mechanisms.

Data availability

No primary research results, software or code have been included and no new data were generated or analysed as part of this review.

Author contributions

Conceptualization: Dongao Zhang, Hua Zhang, and Jian-Feng Li. Validation: Dongao Zhang, Hua Zhang, and Jian-Feng Li. Resources: Hua Zhang and Jian-Feng Li. Writing – original draft: Dongao Zhang, Xuan Liu and Yu Zhao. Writing – review & editing: Dongao Zhang, Xuan Liu, Yu Zhao, Hua Zhang, Alexander V. Rudnev, and Jian-Feng Li. Visualization: Dongao Zhang, Hua Zhang, and Jian-Feng Li. Supervision: Hua Zhang and Jian-Feng Li.

Conflicts of interest

There are no conflicts to declare.

Acknowledgements

This work was supported by the National Key Research and Development Program of China (2022YFA1503800), the National Natural Science Foundation of China (22361132532, 22302163, 22102136, 52171222, and T2293692), "111" Project (B17027), the Fundamental Research Funds for the Central Universities (20720240054), the State Key Laboratory of Fine Chemicals at Dalian University of Technology (KF2401), and NFFTBS (No. J1310024). AR acknowledges financial support from the Russian Science Foundation (project no. 24-43-00142, https://www.rscf.ru/project/24-43-00142/).

Notes and references

1 R. Li, K. Xiang, Z. Peng, Y. Zou and S. Wang, Recent Advances on Electrolysis for Simultaneous Generation of Valuable Chemicals at both Anode and Cathode, *Adv. Energy Mater.*, 2021, **11**, 2102292.
2 S. Xu and E. A. Carter, Theoretical Insights into Heterogeneous (Photo)electrochemical CO_2 Reduction, *Chem. Rev.*, 2019, **119**, 6631–6669.
3 T. Zheng, K. Jiang and H. Wang, Recent Advances in Electrochemical CO_2-to-CO Conversion on Heterogeneous Catalysts, *Adv. Mater.*, 2018, **30**, 1802066.
4 J. Yu, J. Wang, Y. Ma, J. Zhou, Y. Wang, P. Lu, J. Yin, R. Ye, Z. Zhu and Z. Fan, Recent Progresses in Electrochemical Carbon Dioxide Reduction on Copper-Based Catalysts toward Multicarbon Products, *Adv. Funct. Mater.*, 2021, **31**, 2102151.
5 A. Liu, M. Gao, X. Ren, F. Meng, Y. Yang, L. Gao, Q. Yang and T. Ma, Current progress in electrocatalytic carbon dioxide reduction to fuels on heterogeneous catalysts, *J. Mater. Chem. A*, 2020, **8**, 3541–3562.
6 X. Chang, T. Wang, P. Yang, G. Zhang and J. Gong, The Development of Cocatalysts for Photoelectrochemical CO_2 Reduction, *Adv. Mater.*, 2019, **31**, 1804710.
7 L. C. Banerji, H. Jang, A. M. Gardner and A. J. Cowan, Studying the cation dependence of CO_2 reduction intermediates at Cu by *in situ* VSFG spectroscopy, *Chem. Sci.*, 2024, **15**, 2889–2897.
8 Z. Sun, T. Ma, H. Tao, Q. Fan and B. Han, Fundamentals and Challenges of Electrochemical CO_2 Reduction Using Two-Dimensional Materials, *Chem*, 2017, **3**, 560–587.
9 Y. Song, X. Zhang, K. Xie, G. Wang and X. Bao, High-Temperature CO_2 Electrolysis in Solid Oxide Electrolysis Cells: Developments, Challenges, and Prospects, *Adv. Mater.*, 2019, **31**, 1902033.
10 I. Sullivan, A. Goryachev, I. A. Digdaya, X. Li, H. A. Atwater, D. A. Vermaas and C. Xiang, Coupling electrochemical CO_2 conversion with CO_2 capture, *Nat. Catal.*, 2021, **4**, 952–958.
11 R. Shi, J. Guo, X. Zhang, G. I. N. Waterhouse, Z. Han, Y. Zhao, L. Shang, C. Zhou, L. Jiang and T. Zhang, Efficient wettability-controlled electroreduction of CO_2 to CO at Au/C interfaces, *Nat. Commun.*, 2020, **11**, 3028.
12 C. Rogers, W. S. Perkins, G. Veber, T. E. Williams, R. R. Cloke and F. R. Fischer, Synergistic Enhancement of Electrocatalytic CO_2 Reduction with Gold Nanoparticles Embedded in Functional Graphene Nanoribbon Composite Electrodes, *J. Am. Chem. Soc.*, 2017, **139**, 4052–4061.
13 Y. Lu, L. Zhou, S. Wang and Y. Zou, Defect engineering of electrocatalysts for organic synthesis, *Nano Res.*, 2023, **16**, 1890–1912.
14 T. Ma, Z. Jiao, H. Qiu, F. Wang, Y. Liu and L. Guo, Synergistic effect of oxygen species and vacancy for

enhanced electrochemical CO_2 conversion to formate on indium oxide, *eScience*, 2024, **4**, 100246.

15 S. Y. Lee, H. Jung, N.-K. Kim, H.-S. Oh, B. K. Min and Y. J. Hwang, Mixed Copper States in Anodized Cu Electrocatalyst for Stable and Selective Ethylene Production from CO_2 Reduction, *J. Am. Chem. Soc.*, 2018, **140**, 8681–8689.

16 Y. Yang, M. Z. Ertem and L. Duan, An amide-based second coordination sphere promotes the dimer pathway of Mn-catalyzed CO_2-to-CO reduction at low overpotential, *Chem. Sci.*, 2021, **12**, 4779–4788.

17 W. Nie, G. P. Heim, N. B. Watkins, T. Agapie and J. C. Peters, Organic Additive-derived Films on Cu Electrodes Promote Electrochemical CO_2 Reduction to C_{2+} Products Under Strongly Acidic Conditions, *Angew. Chem., Int. Ed.*, 2023, **135**, e202216102.

18 J. Li, Y. Kuang, Y. Meng, X. Tian, W.-H. Hung, X. Zhang, A. Li, M. Xu, W. Zhou, C.-S. Ku, C.-Y. Chiang, G. Zhu, J. Guo, X. Sun and H. Dai, Electroreduction of CO_2 to Formate on a Copper-Based Electrocatalyst at High Pressures with High Energy Conversion Efficiency, *J. Am. Chem. Soc.*, 2020, **142**, 7276–7282.

19 H. H. Wong, M. Sun, T. Wu, C. H. Chan, L. Lu, Q. Lu, B. Chen and B. Huang, Neighboring effect in single-atom catalysts for the electrochemical carbon dioxide reduction reaction, *eScience*, 2024, **4**, 100140.

20 F. Chen, Z.-C. Yao, Z.-H. Lyu, J. Fu, X. Zhang and J.-S. Hu, Recent advances in p-block metal chalcogenide electrocatalysts for high-efficiency CO_2 reduction, *eScience*, 2024, **4**, 100172.

21 S. Lin, C. S. Diercks, Y.-B. Zhang, N. Kornienko, E. M. Nichols, Y. Zhao, A. R. Paris, D. Kim, P. Yang, O. M. Yaghi and C. J. Chang, Covalent organic frameworks comprising cobalt porphyrins for catalytic CO_2 reduction in water, *Science*, 2015, **349**, 1208–1213.

22 C. Y. J. Lim, M. Yilmaz, J. M. Arce-Ramos, A. D. Handoko, W. J. Teh, Y. Zheng, Z. H. J. Khoo, M. Lin, M. Isaacs, T. L. D. Tam, Y. Bai, C. K. Ng, B. S. Yeo, G. Sankar, I. P. Parkin, K. Hippalgaonkar, M. B. Sullivan, J. Zhang and Y.-F. Lim, Surface charge as activity descriptors for electrochemical CO_2 reduction to multi-carbon products on organic-functionalised Cu, *Nat. Commun.*, 2023, **14**, 335.

23 Y. Jia, K. Jiang, H. Wang and X. Yao, The Role of Defect Sites in Nanomaterials for Electrocatalytic Energy Conversion, *Chem*, 2019, **5**, 1371–1397.

24 J. Hussain, H. Jonsson and E. Skulason, Calculations of Product Selectivity in Electrochemical CO_2 Reduction, *ACS Catal.*, 2018, **8**, 5240–5249.

25 J. Huang, M. Mensi, E. Oveisi, V. Mantella and R. Buonsanti, Structural Sensitivities in Bimetallic Catalysts for Electrochemical CO_2 Reduction Revealed by Ag-Cu Nanodimers, *J. Am. Chem. Soc.*, 2019, **141**, 2490–2499.

26 S. Liu, J. Xiao, X. F. Lu, J. Wang, X. Wang and X. W. Lou, Efficient Electrochemical Reduction of CO_2 to HCOOH over Sub-2nm SnO_2 Quantum Wires with Exposed Grain Boundaries, *Angew. Chem., Int. Ed.*, 2019, **58**, 8499–8503.

27 M. C. O. Monteiro, S. Dieckhoefer, T. Bobrowski, T. Quast, D. Pavesi, M. T. M. Koper and W. Schuhmann, Probing the local activity of CO_2 reduction on gold gas diffusion electrodes: effect of the catalyst loading and CO_2 pressure, *Chem. Sci.*, 2021, **12**, 15682–15690.

28 H. Bao, S. X. Leong, J. R. T. Chen, Z. Shi, S. Chen, Y. Lv, T. Liu, I. Y. Phang and X. Y. Ling, Advancing Energy Systems with *In-Situ* and Operando Surface-Enhanced Raman Scattering Spectroscopy, *CCS Chem.*, 2024, **6**, 1403–1421.

29 T. N. Nguyen and C.-T. Dinh, Gas diffusion electrode design for electrochemical carbon dioxide reduction, *Chem. Soc. Rev.*, 2020, **49**, 7488–7504.

30 J. Li, G. Chen, Y. Zhu, Z. Liang, A. Pei, C.-L. Wu, H. Wang, H. R. Lee, K. Liu, S. Chu and Y. Cui, Efficient electrocatalytic CO_2 reduction on a three-phase interface, *Nat. Catal.*, 2018, **1**, 592–600.

31 D. Wenlong and L. I. U. Luqi, Recent Advances of Raman Spectroscopy in Structural Characterization of Two-dimensional Materials, *Chin. J. Light Scattering*, 2021, **33**, 1–15.

32 S. I. Lifang, F. A. N. Xingce, H. O. U. Xiangyu, L. I. Guoqun, L. Kailin, L. U. O. Xiaoguang, N. I. Zhenhua and Q. I. U. Teng, Assembly of Indium Tin Oxide Nanoarrays for Synergistically Enhanced Raman Scattering, *Chin. J. Light Scattering*, 2021, **33**, 32–39.

33 L. Han Cong, Development progress of miniaturized Raman spectrometers, *Chin. J. Light Scattering*, 2024, **36**, 260–270.

34 Y. J.-l. Shi Can, *In-situ* SERS Studies on the Degradation of Methyl Orange at Cu_2O-Au Composites Surfaces, *Chin. J. Light Scattering*, 2023, **35**, 391–398.

35 Y.-H. Wang, S. Zheng, W.-M. Yang, R.-Y. Zhou, Q.-F. He, P. Radjenovic, J.-C. Dong, S. Li, J. Zheng, Z.-L. Yang, G. Attard, F. Pan, Z.-Q. Tian and J.-F. Li, *In situ* Raman spectroscopy reveals the structure and dissociation of interfacial water, *Nature*, 2021, **600**, 81–85.

36 J.-C. Dong, X.-G. Zhang, V. Briega-Martos, X. Jin, J. Yang, S. Chen, Z.-L. Yang, D.-Y. Wu, J. M. Feliu, C. T. Williams, Z.-Q. Tian and J.-F. Li, *In situ* Raman spectroscopic evidence for oxygen reduction reaction intermediates at platinum single-crystal surfaces, *Nat. Energy*, 2019, **4**, 60–67.

37 J. F. Li, Y. F. Huang, Y. Ding, Z. L. Yang, S. B. Li, X. S. Zhou, F. R. Fan, W. Zhang, Z. Y. Zhou, D. Y. Wu, B. Ren, Z. L. Wang and Z. Q. Tian, Shell-isolated nanoparticle-enhanced Raman spectroscopy, *Nature*, 2010, **464**, 392–395.

38 H. Zhang, C. Wang, H.-L. Sun, G. Fu, S. Chen, Y.-J. Zhang, B.-H. Chen, J. R. Anema, Z.-L. Yang, J.-F. Li and Z.-Q. Tian, *In situ* dynamic tracking of heterogeneous nanocatalytic processes by shell-isolated nanoparticle-enhanced Raman spectroscopy, *Nat. Commun.*, 2017, **8**, 15447.

39 X. You, D. Zhang, X.-G. Zhang, X. Li, J.-H. Tian, Y.-H. Wang and J.-F. Li, Exploring the Cation Regulation Mechanism for Interfacial Water Involved in the Hydrogen Evolution

Reaction by *In Situ* Raman Spectroscopy, *Nano-Micro Lett.*, 2024, **16**, 53.

40 M. Li, Y. Ma, J. Chen, R. Lawrence, W. Luo, M. Sacchi, W. Jiang and J. Yang, Residual Chlorine Induced Cationic Active Species on a Porous Copper Electrocatalyst for Highly Stable Electrochemical CO_2 Reduction to C_{2+}, *Angew. Chem., Int. Ed.*, 2021, **60**, 11487–11493.

41 J. Jiao, R. Lin, S. Liu, W.-C. Cheong, C. Zhang, Z. Chen, Y. Pan, J. Tang, K. Wu, S.-F. Hung, H. M. Chen, L. Zheng, Q. Lu, X. Yang, B. Xu, H. Xiao, J. Li, D. Wang, Q. Peng, C. Chen and Y. Li, Copper atom-pair catalyst anchored on alloy nanowires for selective and efficient electrochemical reduction of CO_2, *Nat. Chem.*, 2019, **11**, 222–228.

42 X. Chang, J. Li, H. Xiong, H. Zhang, Y. Xu, H. Xiao, Q. Lu and B. Xu, C-C Coupling Is Unlikely to Be the Rate-Determining Step in the Formation of C_{2+} Products in the Copper-Catalyzed Electrochemical Reduction of CO, *Angew. Chem., Int. Ed.*, 2022, **61**, e202111167.

43 T.-C. Chou, C.-C. Chang, H.-L. Yu, W.-Y. Yu, C.-L. Dong, J. J. Velasco-Velez, C.-H. Chuang, L.-C. Chen, J.-F. Lee, J.-M. Chen and H.-L. Wu, Controlling the Oxidation State of the Cu Electrode and Reaction Intermediates for Electrochemical CO_2 Reduction to Ethylene, *J. Am. Chem. Soc.*, 2020, **142**, 2857–2867.

44 W. Zhu, Y.-J. Zhang, H. Zhang, H. Lv, Q. Li, R. Michalsky, A. A. Peterson and S. Sun, Active and Selective Conversion of CO_2 to CO on Ultrathin Au Nanowires, *J. Am. Chem. Soc.*, 2014, **136**, 16132–16135.

45 A. Bagger, W. Ju, A. Sofia Varela, P. Strasser and J. Rossmeisl, Electrochemical CO_2 Reduction: A Classification Problem, *ChemPhysChem*, 2017, **18**, 3266–3273.

46 S. Nitopi, E. Bertheussen, S. B. Scott, X. Liu, A. K. Engstfeld, S. Horch, B. Seger, I. E. L. Stephens, K. Chan, C. Hahn, J. K. Norskov, T. F. Jaramillo and I. Chorkendorff, Progress and Perspectives of Electrochemical CO_2 Reduction on Copper in Aqueous Electrolyte, *Chem. Rev.*, 2019, **119**, 7610–7672.

47 N. Han, P. Ding, L. He, Y. Li and Y. Li, Promises of Main Group Metal-Based Nanostructured Materials for Electrochemical CO_2 Reduction to Formate, *Adv. Energy Mater.*, 2020, **10**, 1902338.

48 Z.-H. Gao, K. Wei, T. Wu, J. Dong, D.-E. Jiang, S. Sun and L.-S. Wang, A Heteroleptic Gold Hydride Nanocluster for Efficient and Selective Electrocatalytic Reduction of CO_2 to CO, *J. Am. Chem. Soc.*, 2022, **144**, 5258–5262.

49 K. Ye, Z. Zhou, J. Shao, L. Lin, D. Gao, N. Ta, R. Si, G. Wang and X. Bao, *In Situ* Reconstruction of a Hierarchical Sn-Cu/SnO_x Core/Shell Catalyst for High-Performance CO_2 Electroreduction, *Angew. Chem., Int. Ed.*, 2020, **59**, 4814–4821.

50 J. M. Li, F. F. Li, C. Liu, F. Y. Wei, J. Gong, W. Z. Li, L. W. Xue, J. L. Yin, L. Xiao, G. W. Wang, J. T. Lu and L. Zhuang, Polyquinone Modification Promotes CO_2 Activation and Conversion to C_{2+} Products over Copper Electrode, *ACS Energy Lett.*, 2022, **7**, 4045–4051.

51 X. Chang, Y. Zhao and B. Xu, pH Dependence of Cu Surface Speciation in the Electrochemical CO Reduction Reaction, *ACS Catal.*, 2020, **10**, 13737–13747.

52 N. Han, Y. Wang, L. Ma, J. Wen, J. Li, H. Zheng, K. Nie, X. Wang, F. Zhao, Y. Li, J. Fan, J. Zhong, T. Wu, D. J. Miller, J. Lu, S.-T. Lee and Y. Li, Supported Cobalt Polyphthalocyanine for High-Performance Electrocatalytic CO_2 Reduction, *Chem*, 2017, **3**, 652–664.

53 Y. Cai, J. Fu, Y. Zhou, Y.-C. Chang, Q. Min, J.-J. Zhu, Y. Lin and W. Zhu, Insights on forming N,O-coordinated Cu single-atom catalysts for electrochemical reduction CO_2 to methane, *Nat. Commun.*, 2021, **12**, 586.

54 N. Zhang, X. Zhang, L. Tao, P. Jiang, C. Ye, R. Lin, Z. Huang, A. Li, D. Pang, H. Yan, Y. Wang, P. Xu, S. An, Q. Zhang, L. Liu, S. Du, X. Han, D. Wang and Y. Li, Silver Single-Atom Catalyst for Efficient Electrochemical CO_2 Reduction Synthesized from Thermal Transformation and Surface Reconstruction, *Angew. Chem., Int. Ed.*, 2021, **60**, 6170–6176.

55 J. Yin, Z. Gao, F. Wei, C. Liu, J. Gong, J. Li, W. Li, L. Xiao, G. Wang, J. Lu and L. Zhuang, Customizable CO_2 Electroreduction to C_1 or C_{2+} Products through Cu_y/CeO_2 Interface Engineering, *ACS Catal.*, 2022, **12**, 1004–1011.

56 Z. Li, Y. Yang, Z. Yin, X. Wei, H. Peng, K. Lyu, F. Wei, L. Xiao, G. Wang, H. D. Abruna, J. Lu and L. Zhuang, Interface-Enhanced Catalytic Selectivity on the C_2 Products of CO_2 Electroreduction, *ACS Catal.*, 2021, **11**, 2473–2482.

57 M. Li, H. Wang, W. Luo, P. C. Sherrell, J. Chen and J. Yang, Heterogeneous Single-Atom Catalysts for Electrochemical CO_2 Reduction Reaction, *Adv. Mater.*, 2020, **32**, 2001848.

58 H. Rabiee, L. Ge, X. Zhang, S. Hu, M. Li and Z. Yuan, Gas diffusion electrodes (GDEs) for electrochemical reduction of carbon dioxide, carbon monoxide, and dinitrogen to value-added products: a review, *Energy Environ. Sci.*, 2021, **14**, 1959–2008.

59 B. Huang, X. Wang, W. Li, W. Tian, L. Luo, X. Sun, G. Wang, L. Zhuang and L. Xiao, Accelerating Gas Escape in Anion Exchange Membrane Water Electrolysis by Gas Diffusion Layers with Hierarchical Grid Gradients, *Angew. Chem., Int. Ed.*, 2023, **62**, e202304230.

60 W. W. Guo, X. X. Tan, J. H. Bi, L. Xu, D. X. Yang, C. J. Chen, Q. G. Zhu, J. Ma, A. Tayal, J. Y. Ma, Y. Y. Huang, X. F. Sun, S. J. Liu and B. X. Han, Atomic Indium Catalysts for Switching CO_2 Electroreduction Products from Formate to CO, *J. Am. Chem. Soc.*, 2021, **143**, 6877–6885.

61 E. W. Lees, B. A. W. Mowbray, F. G. L. Parlane and C. P. Berlinguette, Gas diffusion electrodes and membranes for CO_2 reduction electrolysers, *Nat. Rev. Mater.*, 2022, **7**, 55–64.

62 X. Tan, K. Sun, Z. Zhuang, B. Hu, Y. Zhang, Q. Liu, C. He, Z. Xu, C. Chen, H. Xiao and C. Chen, Stabilizing Copper by a Reconstruction-Resistant Atomic Cu-O-Si Interface for Electrochemical CO_2 Reduction, *J. Am. Chem. Soc.*, 2023, **145**, 8656–8664.

63 M. G. Kibria, J. P. Edwards, C. M. Gabardo, D. Cao-Thang, A. Seifitokaldani, D. Sinton and E. H. Sargent, Electrochemical CO_2 Reduction into Chemical Feedstocks:

From Mechanistic Electrocatalysis Models to System Design, *Adv. Mater.*, 2019, **31**, 1807166.

64 C. Kim, J. C. Bui, X. Luo, J. K. Cooper, A. Kusoglu, A. Z. Weber and A. T. Bell, Tailored catalyst microenvironments for CO_2 electroreduction to multicarbon products on copper using bilayer ionomer coatings, *Nat. Energy*, 2021, **6**, 1026–1034.

65 Y. C. Tan, K. B. Lee, H. Song and J. Oh, Modulating Local CO_2 Concentration as a General Strategy for Enhancing C-C Coupling in CO_2 Electroreduction, *Joule*, 2020, **4**, 1104–1120.

66 X. Li, L. Liu, X. Ren, J. Gao, Y. Huang and B. Liu, Microenvironment modulation of single-atom catalysts and their roles in electrochemical energy conversion, *Sci. Adv.*, 2020, **6**, eabb6833.

67 M. Wang and J. Luo, A coupled electrochemical system for CO_2 capture, conversion and product purification, *eScience*, 2023, **3**, 100155.

68 X. Wang, J. F. de Araujo, W. Ju, A. Bagger, H. Schmies, S. Kuhl, J. Rossmeisl and P. Strasser, Mechanistic reaction pathways of enhanced ethylene yields during electroreduction of CO_2-CO co-feeds on Cu and Cu-tandem electrocatalysts, *Nat. Nanotechnol.*, 2019, **14**, 1063–1070.

69 Y. Deng, J. Zhao, S. Wang, R. Chen, J. Ding, H.-J. Tsai, W.-J. Zeng, S.-F. Hung, W. Xu, J. Wang, F. Jaouen, X. Li, Y. Huang and B. Liu, Operando Spectroscopic Analysis of Axial Oxygen-Coordinated Single-Sn-Atom Sites for Electrochemical CO_2 Reduction, *J. Am. Chem. Soc.*, 2023, **145**, 7242–7251.

70 W. Bi, X. Li, R. You, M. Chen, R. Yuan, W. Huang, X. Wu, W. Chu, C. Wu and Y. Xie, Surface Immobilization of Transition Metal Ions on Nitrogen-Doped Graphene Realizing High-Efficient and Selective CO_2 Reduction, *Adv. Mater.*, 2018, **30**, 1706617.

71 X. Qin, T. Vegge and H. A. Hansen, Cation-Coordinated Inner-Sphere CO_2 Electroreduction at Au-Water Interfaces, *J. Am. Chem. Soc.*, 2023, **145**, 1897–1905.

72 C. Zhang, S. Yang, J. Wu, M. Liu, S. Yazdi, M. Ren, J. Sha, J. Zhong, K. Nie, A. S. Jalilov, Z. Li, H. Li, B. I. Yakobson, Q. Wu, E. Ringe, H. Xu, P. M. Ajayan and J. M. Tour, Electrochemical CO_2 Reduction with Atomic Iron-Dispersed on Nitrogen-Doped Graphene, *Adv. Energy Mater.*, 2018, **8**, 1703487.

73 S. Chatterjee, I. Dutta, Y. Lum, Z. Lai and K.-W. Huang, Enabling storage and utilization of low-carbon electricity: power to formic acid, *Energy Environ. Sci.*, 2021, **14**, 1194–1246.

74 Z. Zhao and G. Lu, Circumventing the scaling relationship on bimetallic monolayer electrocatalysts for selective CO_2 reduction, *Chem. Sci.*, 2022, **13**, 3880–3887.

75 S. Yang, H. An, S. Arnouts, H. Wang, X. Yu, J. de Ruiter, S. Bals, T. Altantzis, B. M. Weckhuysen and W. van der Stam, Halide-guided active site exposure in bismuth electrocatalysts for selective CO_2 conversion into formic acid, *Nat. Catal.*, 2023, **6**, 796–806.

76 Z. Gu, H. Shen, Z. Chen, Y. Yang, C. Yang, Y. Ji, Y. Wang, C. Zhu, J. Liu, J. Li, T.-K. Sham, X. Xu and G. Zheng, Efficient Electrocatalytic CO_2 Reduction to C_{2+} Alcohols at Defect-Site-Rich Cu Surface, *Joule*, 2021, **5**, 429–440.

77 T. Wang, J. Chen, X. Ren, J. Zhang, J. Ding, Y. Liu, K. H. Lim, J. Wang, X. Li, H. Yang, Y. Huang, S. Kawi and B. Liu, Halogen-Incorporated Sn Catalysts for Selective Electrochemical CO_2 Reduction to Formate, *Angew. Chem., Int. Ed.*, 2023, **62**, e202211174.

78 Z.-Y. Du, K. Wang, S.-B. Li, Y.-M. Xie, J.-H. Tian, Q.-N. Zheng, W. F. Ip, H. Zhang, J.-F. Li and Z.-Q. Tian, *In Situ* Raman Spectroscopic Studies of Electrochemical CO_2 Reduction on Cu-Based Electrodes, *J. Phys. Chem. C*, 2024, **128**, 11741–11755.

79 H.-S. Su, X. Chang and B. Xu, Surface-enhanced vibrational spectroscopies in electrocatalysis: Fundamentals, challenges, and perspectives, *Chin. J. Catal.*, 2022, **43**, 2757–2771.

80 Z. Xia, C. Ma, Y. Fan, Y. Lu, Y.-C. Huang, Y. Pan, Y. Wu, Q. Luo, Y. He, C.-L. Dong, S. Wang and Y. Zou, Vacancy Optimized Coordination on Nickel Oxide for Selective Electrocatalytic Oxidation of Glycerol, *ACS Catal.*, 2024, **14**, 1930–1938.

81 X. Chang, S. Vijay, Y. Zhao, N. J. Oliveira, K. Chan and B. Xu, Understanding the complementarities of surface-enhanced infrared and Raman spectroscopies in CO adsorption and electrochemical reduction, *Nat. Commun.*, 2022, **13**, 2656.

82 E. X. Tan, S. X. Leong, W. A. Liew, I. Y. Phang, J. Y. Ng, N. S. Tan, Y. H. Lee and X. Y. Ling, Forward-predictive SERS-based chemical taxonomy for untargeted structural elucidation of epimeric cerebrosides, *Nat. Commun.*, 2024, **15**, 2582.

83 R. G. Mariano, K. McKelvey, H. S. White and M. W. Kanan, Selective increase in CO_2 electroreduction activity at grain-boundary surface terminations, *Science*, 2017, **358**, 1187–1191.

84 Y. Ouyang, L. Shi, X. Bai, Q. Li and J. Wang, Breaking scaling relations for efficient CO_2 electrochemical reduction through dual-atom catalysts, *Chem. Sci.*, 2020, **11**, 1807–1813.

85 J. Li, H. Zeng, X. Dong, Y. Ding, S. Hu, R. Zhang, Y. Dai, P. Cui, Z. Xiao, D. Zhao, L. Zhou, T. Zheng, J. Xiao, J. Zeng and C. Xia, Selective CO_2 electrolysis to CO using isolated antimony alloyed copper, *Nat. Commun.*, 2023, **14**, 340.

86 M. Ma, K. Djanashvili and W. A. Smith, Controllable Hydrocarbon Formation from the Electrochemical Reduction of CO_2 over Cu Nanowire Arrays, *Angew. Chem., Int. Ed.*, 2016, **55**, 6680–6684.

87 M. Fan, J. E. Huang, R. K. Miao, Y. Mao, P. Ou, F. Li, X.-Y. Li, Y. Cao, Z. Zhang, J. Zhang, Y. Yan, A. Ozden, W. Ni, Y. Wang, Y. Zhao, Z. Chen, B. Khatir, C. P. O'Brien, Y. Xu, Y. C. Xiao, G. I. N. Waterhouse, K. Golovin, Z. Wang, E. H. Sargent and D. Sinton, Cationic-group-functionalized electrocatalysts enable stable acidic CO_2 electrolysis, *Nat. Catal.*, 2023, **6**, 763–772.

88 T. Tang, Z. Wang and J. Guan, Optimizing the Electrocatalytic Selectivity of Carbon Dioxide Reduction Reaction by Regulating the Electronic Structure of Single-Atom M-N-C Materials, *Adv. Funct. Mater.*, 2022, **32**, 2111504.

89 Z. Wu, H. Wu, W. Cai, Z. Wen, B. Jia, L. Wang, W. Jin and T. Ma, Engineering Bismuth-Tin Interface in Bimetallic Aerogel with a 3D Porous Structure for Highly Selective Electrocatalytic CO_2 Reduction to HCOOH, *Angew. Chem., Int. Ed.*, 2021, **60**, 12554–12559.

90 S. Yang, M. Jiang, W. Zhang, Y. Hu, J. Liang, Y. Wang, Z. Tie and Z. Jin, *In Situ* Structure Refactoring of Bismuth Nanoflowers for Highly Selective Electrochemical Reduction of CO_2 to Formate, *Adv. Funct. Mater.*, 2023, **33**, 2301984.

91 A. D. Handoko, F. X. Wei, Jenndy, B. S. Yeo and Z. W. Seh, Understanding heterogeneous electrocatalytic carbon dioxide reduction through operando techniques, *Nat. Catal.*, 2018, **1**, 922–934.

92 L. Lin, X. He, X.-G. Zhang, W. Ma, B. Zhang, D. Wei, S. Xie, Q. Zhang, X. Yi and Y. Wang, A Nanocomposite of Bismuth Clusters and $Bi_2O_2CO_3$ Sheets for Highly Efficient Electrocatalytic Reduction of CO_2 to Formate, *Angew. Chem., Int. Ed.*, 2023, **62**, e202214959.

93 D. Z. Yao, C. Tang, A. Vasileff, X. Zhi, Y. Jiao and S. Z. Qiao, The Controllable Reconstruction of Bi-MOFs for Electrochemical CO_2 Reduction through Electrolyte and Potential Mediation, *Angew. Chem., Int. Ed.*, 2021, **60**, 18178–18184.

94 A. Dutta, I. Z. Montiel, K. Kiran, A. Rieder, V. Grozovski, L. Gut and P. Broekmann, A Tandem ($Bi_2O_3 \rightarrow Bi_{met}$) Catalyst for Highly Efficient ec-CO_2 Conversion into Formate: Operando Raman Spectroscopic Evidence for a Reaction Pathway Change, *ACS Catal.*, 2021, **11**, 4988–5003.

95 W. Luc, C. Collins, S. Wang, H. Xin, K. He, Y. Kang and F. Jiao, Ag-Sn Bimetallic Catalyst with a Core-Shell Structure for CO_2 Reduction, *J. Am. Chem. Soc.*, 2017, **139**, 1885–1893.

96 J. Pei, T. Wang, R. Sui, X. Zhang, D. Zhou, F. Qin, X. Zhao, Q. Liu, W. Yan, J. Dong, L. Zheng, A. Li, J. Mao, W. Zhu, W. Chen and Z. Zhuang, N-Bridged Co-N-Ni: new bimetallic sites for promoting electrochemical CO_2 reduction, *Energy Environ. Sci.*, 2021, **14**, 3019–3028.

97 J. Hao, Z. Zhuang, J. Hao, K. Cao, Y. Hu, W. Wu, S. Lu, C. Wang, N. Zhang, D. Wang, M. Du and H. Zhu, Strain Relaxation in Metal Alloy Catalysts Steers the Product Selectivity of Electrocatalytic CO_2 Reduction, *ACS Nano*, 2022, **16**, 3251–3263.

98 Y. Song, J. R. C. Junqueira, N. Sikdar, D. Öhl, S. Dieckhöfer, T. Quast, S. Seisel, J. Masa, C. Andronescu and W. Schuhmann, B-Cu-Zn Gas Diffusion Electrodes for CO_2 Electroreduction to C_{2+} Products at High Current Densities, *Angew. Chem., Int. Ed.*, 2021, **60**, 9135–9141.

99 X. Li, S. Wang, L. Li, Y. Sun and Y. Xie, Progress and Perspective for *In Situ* Studies of CO_2 Reduction, *J. Am. Chem. Soc.*, 2020, **142**, 9567–9581.

100 B. Ren, G. Wen, R. Gao, D. Luo, Z. Zhang, W. Qiu, Q. Ma, X. Wang, Y. Cui, L. Ricardez-Sandoval, A. Yu and Z. Chen, Nano-crumples induced Sn-Bi bimetallic interface pattern with moderate electron bank for highly efficient CO_2 electroreduction, *Nat. Commun.*, 2022, **13**, 2486.

101 Y. Y. Birdja, E. Perez-Gallent, M. C. Figueiredo, A. J. Gottle, F. Calle-Vallejo and M. T. M. Koper, Advances and challenges in understanding the electrocatalytic conversion of carbon dioxide to fuels, *Nat. Energy*, 2019, **4**, 732–745.

102 S. Liu, H. B. Yang, S.-F. Hung, J. Ding, W. Cai, L. Liu, J. Gao, X. Li, X. Ren, Z. Kuang, Y. Huang, T. Zhang and B. Liu, Elucidating the Electrocatalytic CO_2 Reduction Reaction over a Model Single-Atom Nickel Catalyst, *Angew. Chem., Int. Ed.*, 2020, **59**, 798–803.

103 S. A. Krasnikov, A. B. Preobrajenski, N. N. Sergeeva, M. M. Brzhezinskaya, M. A. Nesterov, A. A. Cafolla, M. O. Senge and A. S. Vinogradov, Electronic structure of Ni(II) porphyrins and phthalocyanine studied by soft X-ray absorption spectroscopy, *Chem. Phys.*, 2007, **332**, 318–324.

104 Z. Q. Liu, Z. X. Chen, B. B. Jin and X. X. Zhang, Theoretical studies on the structures and vibrational spectra of Ni, Pd, and Pt phthalocyanines, *Vib. Spectrosc.*, 2011, **56**, 210–218.

105 L. Jiao, J. Zhu, Y. Zhang, W. Yang, S. Zhou, A. Li, C. Xie, X. Zheng, W. Zhou, S.-H. Yu and H.-L. Jiang, Non-Bonding Interaction of Neighboring Fe and Ni Single-Atom Pairs on MOF-Derived N-Doped Carbon for Enhanced CO_2 Electroreduction, *J. Am. Chem. Soc.*, 2021, **143**, 19417–19424.

106 Y. Zhang, L. Jiao, W. Yang, C. Xie and H.-L. Jiang, Rational Fabrication of Low-Coordinate Single-Atom Ni Electrocatalysts by MOFs for Highly Selective CO_2 Reduction, *Angew. Chem., Int. Ed.*, 2021, **60**, 7607–7611.

107 L. Jiao, W. Yang, G. Wan, R. Zhang, X. Zheng, H. Zhou, S.-H. Yu and H.-L. Jiang, Single-Atom Electrocatalysts from Multivariate Metal-Organic Frameworks for Highly Selective Reduction of CO_2 at Low Pressures, *Angew. Chem., Int. Ed.*, 2020, **59**, 20589–20595.

108 R. Yang, J. Duan, P. Dong, Q. Wen, M. Wu, Y. Liu, Y. Liu, H. Li and T. Zhai, *In Situ* Halogen-Ion Leaching Regulates Multiple Sites on Tandem Catalysts for Efficient CO_2 Electroreduction to C_{2+} Products, *Angew. Chem., Int. Ed.*, 2022, **61**, e202116706.

109 W. Luc, X. Fu, J. Shi, J.-J. Lv, M. Jouny, B. H. Ko, Y. Xu, Q. Tu, X. Hu, J. Wu, Q. Yue, Y. Liu, F. Jiao and Y. Kang, Two-dimensional copper nanosheets for electrochemical reduction of carbon monoxide to acetate, *Nat. Catal.*, 2019, **2**, 423–430.

110 J. Kim, T. Lee, H. D. Jung, M. Kim, J. Eo, B. Kang, H. Jung, J. Park, D. Bae, Y. Lee, S. Park, W. Kim, S. Back, Y. Lee and D.-H. Nam, Vitamin C-induced CO_2 capture enables high-rate ethylene production in CO_2 electroreduction, *Nat. Commun.*, 2024, **15**, 192.

111 J.-F. Li, Y.-J. Zhang, S.-Y. Ding, R. Panneerselvam and Z.-Q. Tian, Core-Shell Nanoparticle-Enhanced Raman Spectroscopy, *Chem. Rev.*, 2017, **117**, 5002–5069.

112 Y. Zhao, X.-G. Zhang, N. Bodappa, W.-M. Yang, Q. Liang, P. M. Radjenovica, Y.-H. Wang, Y.-J. Zhang, J.-C. Dong, Z.-Q. Tian and J.-F. Li, Elucidating electrochemical CO_2 reduction reaction processes on Cu(*hkl*) single-crystal surfaces by *in situ* Raman spectroscopy, *Energy Environ. Sci.*, 2022, **15**, 3968–3977.

113 Y. Huang, A. D. Handoko, P. Hirunsit and B. S. Yeo, Electrochemical Reduction of CO_2 Using Copper Single-Crystal Surfaces: Effects of CO* Coverage on the Selective Formation of Ethylene, *ACS Catal.*, 2017, **7**, 1749–1756.

114 M. C. Figueiredo, I. Ledezma-Yanez and M. T. M. Koper, *In Situ* Spectroscopic Study of CO_2 Electroreduction at Copper Electrodes in Acetonitrile, *ACS Catal.*, 2016, **6**, 2382–2392.

115 I. V. Chernyshova, P. Somasundaran and S. Ponnurangam, On the origin of the elusive first intermediate of CO_2 electroreduction, *Proc. Natl. Acad. Sci. U.S.A.*, 2018, **115**, E9261–E9270.

116 F. Shao, J. K. Wong, Q. H. Low, M. Iannuzzi, J. Li and J. Lan, *In situ* spectroelectrochemical probing of CO redox landscape on copper single-crystal surfaces, *Proc. Natl. Acad. Sci. U.S.A.*, 2022, **119**, e2118166119.

117 C. M. Gunathunge, X. Li, J. Li, R. P. Hicks, V. J. Ovalle and M. M. Waegele, Spectroscopic Observation of Reversible Surface Reconstruction of Copper Electrodes under CO_2 Reduction, *J. Phys. Chem. C*, 2017, **121**, 12337–12344.

118 A. S. Malkani, M. Dunwell and B. Xuo, Operando Spectroscopic Investigations of Copper and Oxide Derived Copper Catalysts for Electrochemical CO Reduction, *ACS Catal.*, 2019, **9**, 474–478.

119 C. Zhan, F. Dattila, C. Rettenmaier, A. Herzog, M. Herran, T. Wagner, F. Scholten, A. Bergmann, N. López and B. Roldan Cuenya, Key intermediates and Cu active sites for CO_2 electroreduction to ethylene and ethanol, *Nat. Energy*, 2024, **9**, 1485–1496.

120 M. Moradzaman and G. Mul, *In Situ* Raman Study of Potential-Dependent Surface Adsorbed Carbonate, CO, OH, and C Species on Cu Electrodes During Electrochemical Reduction of CO_2, *ChemElectroChem*, 2021, **8**, 1478–1485.

121 J. de Ruiter, H. An, L. Wu, Z. Gijsberg, S. Yang, T. Hartman, B. M. Weckhuysen and W. van der Stam, Probing the Dynamics of Low-Overpotential CO_2-to-CO Activation on Copper Electrodes with Time-Resolved Raman Spectroscopy, *J. Am. Chem. Soc.*, 2022, **144**, 15047–15058.

122 Y. Zang, T. Liu, P. Wei, H. Li, Q. Wang, G. Wang and X. Bao, Selective CO_2 Electroreduction to Ethanol over a Carbon-Coated CuO_x Catalyst, *Angew. Chem., Int. Ed.*, 2022, **61**, e202209629.

123 C. Zhan, F. Dattila, C. Rettenmaier, A. Bergmann, S. Kühl, R. García-Muelas, N. López and B. R. Cuenya, Revealing the CO Coverage-Driven C-C Coupling Mechanism for Electrochemical CO_2 Reduction on Cu_2O Nanocubes *via* Operando Raman Spectroscopy, *ACS Catal.*, 2021, **11**, 7694–7701.

124 M. Zheng, P. Wang, X. Zhi, K. Yang, Y. Jiao, J. Duan, Y. Zheng and S.-Z. Qiao, Electrocatalytic CO_2-to-C_{2+} with Ampere-Level Current on Heteroatom-Engineered Copper *via* Tuning *CO Intermediate Coverage, *J. Am. Chem. Soc.*, 2022, **144**, 14936–14944.

125 M. Asadi, K. Kim, C. Liu, A. V. Addepalli, P. Abbasi, P. Yasaei, P. Phillips, A. Behranginia, J. M. Cerrato, R. Haasch, P. Zapol, B. Kumar, R. F. Klie, J. Abiade, L. A. Curtiss and A. Salehi-Khojin, Nanostructured transition metal dichalcogenide electrocatalysts for CO_2 reduction in ionic liquid, *Science*, 2016, **353**, 467–470.

126 A. Ozden, Y. Wang, F. Li, M. Luo, J. Sisler, A. Thevenon, A. Rosas-Hernandez, T. Burdyny, Y. Lum, H. Yadegari, T. Agapie, J. C. Peters, E. H. Sargent and D. Sinton, Cascade CO_2 electroreduction enables efficient carbonate-free production of ethylene, *Joule*, 2021, **5**, 706–719.

127 E. L. Clark, C. Hahn, T. F. Jaramillo and A. T. Bell, Electrochemical CO_2 Reduction over Compressively Strained CuAg Surface Alloys with Enhanced Multi-Carbon Oxygenate Selectivity, *J. Am. Chem. Soc.*, 2017, **139**, 15848–15857.

128 M. Xie, Y. Shen, W. Ma, D. Wei, B. Zhang, Z. Wang, Y. Wang, Q. Zhang, S. Xie, C. Wang and Y. Wang, Fast Screening for Copper-Based Bimetallic Electrocatalysts: Efficient Electrocatalytic Reduction of CO_2 to C_{2+} Products on Magnesium-Modified Copper, *Angew. Chem., Int. Ed.*, 2022, **61**, e202213423.

129 W. Xia, Y. Xie, S. Jia, S. Han, R. Qi, T. Chen, X. Xing, T. Yao, D. Zhou, X. Dong, J. Zhai, J. Li, J. He, D. Jiang, Y. Yamauchi, M. He, H. Wu and B. Han, Adjacent Copper Single Atoms Promote C-C Coupling in Electrochemical CO_2 Reduction for the Efficient Conversion of Ethanol, *J. Am. Chem. Soc.*, 2023, **145**, 17253–17264.

130 C. M. Gunathunge, V. J. Ovalle, Y. Li, M. J. Janik and M. M. Waegele, Existence of an Electrochemically Inert CO Population on Cu Electrodes in Alkaline pH, *ACS Catal.*, 2018, **8**, 7507–7516.

131 G. Shi, Y. Xie, L. Du, X. Fu, X. Chen, W. Xie, T.-B. Lu, M. Yuan and M. Wang, Constructing Cu-C Bonds in a Graphdiyne-Regulated Cu Single-Atom Electrocatalyst for CO_2 Reduction to CH_4, *Angew. Chem., Int. Ed.*, 2022, **61**, e202203569.

132 H. L. Gu, L. X. Zhong, G. S. Shi, J. Q. Li, K. Yu, J. Li, S. Zhang, C. Y. Zhu, S. H. Chen, C. L. Yang, Y. Kong, C. Chen, S. Z. Li, J. Zhang and L. M. Zhang, Graphdiyne/Graphene Heterostructure: A Universal 2D Scaffold Anchoring Monodispersed Transition-Metal Phthalocyanines for Selective and Durable CO_2 Electroreduction, *J. Am. Chem. Soc.*, 2021, **143**, 8679–8688.

133 G. D. Shi, Z. X. Fan, L. L. Du, X. L. Fu, C. M. Dong, W. Xie, D. B. Zhao, M. Wang and M. J. Yuan, *In situ* construction of graphdiyne/CuS heterostructures for efficient hydrogen evolution reaction, *Mater. Chem. Front.*, 2019, **3**, 821–828.

134 G.-Y. Duan, X.-Q. Li, G.-R. Ding, L.-J. Han, B.-H. Xu and S.-J. Zhang, Highly Efficient Electrocatalytic CO_2 Reduction to C_{2+} Products on a Poly(ionic liquid)-Based Cu^0-Cu^I Tandem Catalyst, *Angew. Chem., Int. Ed.*, 2022, **61**, e202110657.

135 Z. Z. Niu, F. Y. Gao, X. L. Zhang, P. P. Yang, R. Liu, L. P. Chi, Z. Z. Wu, S. Qin, X. X. Yu and M. R. Gao, Hierarchical

Copper with Inherent Hydrophobicity Mitigates Electrode Flooding for High-Rate CO_2 Electroreduction to Multicarbon Products, *J. Am. Chem. Soc.*, 2021, **143**, 8011–8021.

136 Y. R. Zhao, X. Z. Chang, A. S. Malkani, X. Yang, L. Thompson, F. Jiao and B. J. Xu, Speciation of Cu Surfaces During the Electrochemical CO Reduction Reaction, *J. Am. Chem. Soc.*, 2020, **142**, 9735–9743.

137 F. Li, Y. C. Li, Z. Wang, J. Li, D.-H. Nam, Y. Lum, M. Luo, X. Wang, A. Ozden, S.-F. Hung, B. Chen, Y. Wang, J. Wicks, Y. Xu, Y. Li, C. M. Gabardo, C.-T. Dinh, Y. Wang, T.-T. Zhuang, D. Sinton and E. H. Sargent, Cooperative CO_2-to-ethanol conversion *via* enriched intermediates at molecule-metal catalyst interfaces, *Nat. Catal.*, 2020, **3**, 75–82.

138 C. Costentin, S. Drouet, G. Passard, M. Robert and J.-M. Savéant, Proton-Coupled Electron Transfer Cleavage of Heavy-Atom Bonds in Electrocatalytic Processes. Cleavage of a C–O Bond in the Catalyzed Electrochemical Reduction of CO_2, *J. Am. Chem. Soc.*, 2013, **135**, 9023–9031.

139 Y. Wang, P. Han, X. Lv, L. Zhang and G. Zheng, Defect and Interface Engineering for Aqueous Electrocatalytic CO_2 Reduction, *Joule*, 2018, **2**, 2551–2582.

140 Z. Cao, D. Kim, D. Hong, Y. Yu, J. Xu, S. Lin, X. Wen, E. M. Nichols, K. Jeong, J. A. Reimer, P. Yang and C. J. Chang, A Molecular Surface Functionalization Approach to Tuning Nanoparticle Electrocatalysts for Carbon Dioxide Reduction, *J. Am. Chem. Soc.*, 2016, **138**, 8120–8125.

141 M. Liu, Y. Pang, B. Zhang, P. De Luna, O. Voznyy, J. Xu, X. Zheng, C. T. Dinh, F. Fan, C. Cao, F. P. G. de Arquer, T. S. Safaei, A. Mepham, A. Klinkova, E. Kumacheva, T. Filleter, D. Sinton, S. O. Kelley and E. H. Sargent, Enhanced electrocatalytic CO_2 reduction *via* field-induced reagent concentration, *Nature*, 2016, **537**, 382–386.

142 W. Q. Gao, Y. F. Xu, L. K. Fu, X. X. Chang and B. J. Xu, Experimental evidence of distinct sites for CO_2-to-CO and CO conversion on Cu in the electrochemical CO_2 reduction reaction, *Nat. Catal.*, 2023, **6**, 885–894.

143 L. B. T. Nguyen, Y. X. Leong, C. S. L. Koh, S. X. Leong, S. K. Boong, H. Y. F. Sim, G. C. Phan-Quang, I. Y. Phang and X. Y. Ling, Inducing Ring Complexation for Efficient Capturing and Detection of Small Gaseous Molecules Using SERS for Environmental Surveillance, *Angew. Chem., Int. Ed.*, 2022, **61**, e202207447.

144 J. E. Huang, F. Li, A. Ozden, A. S. Rasouli, F. P. G. de Arquer, S. Liu, S. Zhang, M. Luo, X. Wang, Y. Lum, Y. Xu, K. Bertens, R. K. Miao, C.-T. Dinh, D. Sinton and E. H. Sargent, CO_2 electrolysis to multicarbon products in strong acid, *Science*, 2021, **372**, 1074–1078.